

Article

Petrogenesis of the Laoshan Suite in the Jiaodong Peninsula (Eastern China): An Oxidized Low Ba–Sr A1-Type Granite

Jian Li ^{1,2,3}, Changwei Wang ^{1,3}, Mingchun Song ^{4,*}, Changjiang Wang ^{1,3}, Shiyong Li ⁵, Xiao Liu ¹ and Qingyi Cui ¹

¹ School of Resources and Environmental Engineering, Shandong University of Technology, Zibo 255049, China; lijian_sdut@163.com (J.L.); wangchangwei_sdut@163.com (C.W.); cj85520819@163.com (C.W.); liuxiaogis@163.com (X.L.); 15265520559@163.com (Q.C.)

² Institute of Geology, Chinese Academy of Geological Sciences, Beijing 100037, China

³ Shandong Zhengyuan Geological Resources Exploration Co., Ltd., Zibo 255049, China

⁴ Hebei Province Collaborative Innovation Center for Strategic Critical Mineral Research, Hebei GEO University, Shijiazhuang 050031, China

⁵ Shandong Province Nuclear Industry Geological Group 273, Yantai 264006, China; dikechulsy@126.com

* Correspondence: mingchuns@163.com; Tel.: +86-137-0531-7191

Abstract: The Jiaodong Peninsula is closely related to Mesozoic granites in terms of spatial and temporal aspects. However, the specific association between the genesis of gold mineralization and these granites remains unclear. It is also ambiguous why Laoshan-type granites, which are similar to Mesozoic granites, are not gold mineralized. In this study, we analyzed the Laoshan granites and compiled Mesozoic magmatic rock data (Linglong, Guojialing, and Weideshan suites) of the Jiaodong Peninsula. We performed whole-rock major and trace elements, LA-ICP-MS zircon U–Pb geochronology and geochemistry analyses. Our zircon U–Pb data denote that the Laoshan granite was emplaced during the 118 ± 1 Ma. The Laoshan granite is characterized by high SiO₂ content (76.03–80.28 wt.%), high TFe₂O₃/MgO (11.1–27.1) and Ga/Al (3.0–3.5) ratios, high zircon saturation temperature (809–850 °C), and negative Eu (Eu/Eu* = 0.05–0.08) anomalies, showing A-type granite characteristics. Furthermore, the Laoshan granite is identified as an A1-type granite with low Ba (33.1–42.0 ppm) and Sr (14.1–21.0 ppm) contents. It was formed in an extensional tectonic environment induced by the subducting slab roll-back of the Paleo-Pacific Plate, mainly from the partial melting of lower crustal materials, mixed with a small amount of mantle components. Zircon trace elements indicate that the Laoshan suite had relatively high oxygen fugacity and temperature ($\Delta FMQ = +2.43$ to $+4.22$, T-Ti in zircon (mean) = 796 °C) compared to the pre-mineralization and contemporaneous mineralization magma. We propose that oxidized adakitic magma (Weideshan suite) may contribute to the enrichment and mineralization of gold. Although Laoshan-type granite also has a high oxygen fugacity, its location is distant from the ore-controlling faults, which ultimately hinders the formation of gold mineralization. From the Jurassic to the Cretaceous, the tectonic and geochemical properties of magmatic rocks in the Jiaodong Peninsula have changed, and gold deposits are formed in such a transitional process (compression to extension, reduction to oxidation).

Keywords: A1-type granite; high oxygen fugacity; adakitic rocks; Laoshan suite; Jiaodong Peninsula



Citation: Li, J.; Wang, C.; Song, M.; Wang, C.; Li, S.; Liu, X.; Cui, Q. Petrogenesis of the Laoshan Suite in the Jiaodong Peninsula (Eastern China): An Oxidized Low Ba–Sr A1-Type Granite. *Minerals* **2023**, *13*, 1012. <https://doi.org/10.3390/min13081012>

Academic Editors: Fan Yang, Cun Zhang, Jian Chang and Jaroslav Dostal

Received: 3 July 2023

Revised: 26 July 2023

Accepted: 26 July 2023

Published: 29 July 2023



Copyright: © 2023 by the authors. Licensee MDPI, Basel, Switzerland. This article is an open access article distributed under the terms and conditions of the Creative Commons Attribution (CC BY) license (<https://creativecommons.org/licenses/by/4.0/>).

1. Introduction

The Jiaodong Peninsula is the world's third-largest gold province, surpassed only by the Witwatersrand Basin in South Africa and the Muruntau in Uzbekistan [1]. Located in the eastern part of the North China Craton (NCC) (Figure 1), the Jiaodong Peninsula hosts a nearly complete record of the complex NCC geological evolution from the Archean to the Cenozoic. Currently, the proven gold reserves in the Jiaodong Peninsula (only 0.3% of Chinese territory) are nearly 6000 t [2], accounting for more than 40% of China's total gold reserves [1,3,4]. Geochronological data from multiple methods (quartz/sericite ⁴⁰Ar/³⁹Ar, pyrite Rb–Sr, and hydrothermal monazite U–Pb) show that the Jiaodong gold deposits were

formed in the late Early Cretaceous (120 ± 5 Ma) [1,3,5–7], with explosive and transient characteristics [8–11]. According to geochronology and geochemical characteristics, the granites in Jiaodong can be divided into Linglong-, Guojialing-, Weideshan-, and Laoshan-type [4]. Previous studies have shown that 80% of gold deposits occur in granite (mainly Linglong and Guojialing) [7]. Although gold mineralization is temporally overlain with Weideshan- and Laoshan-type granites, gold mineralization does not exist in Laoshan-type granites, which are far from gold deposits. It is not yet clear whether the differences in magmatic physicochemical conditions or genetic types have caused the Laoshan-type granite to be unrelated to gold mineralization.

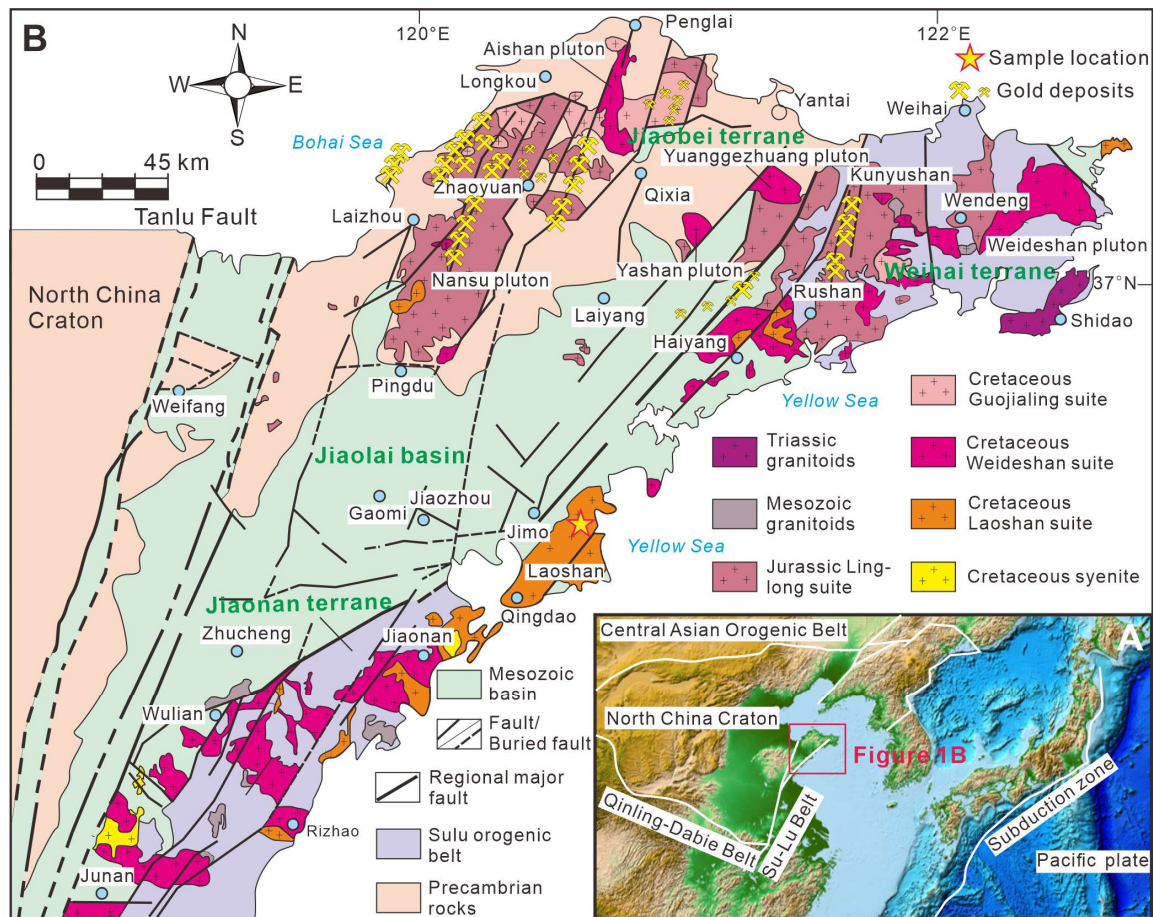


Figure 1. (A). Distribution map of the main tectonic zones in the NCC (after Yang et al. [12]); (B). Detailed geological map of the Jiaodong Peninsula (after Song et al. [4,7]).

To better understand the constraints of Mesozoic magmatic rocks on the formation of gold mineralization in the Jiaodong Peninsula, we present a comprehensive analysis that includes petrographic observations, whole-rock major and trace elements geochemistry data, and the results of laser ablation inductively coupled plasma mass spectrometry (LA-ICP-MS) U–Pb dating of zircon ages and trace elements for the Laoshan suite from the Jiaodong Peninsula. These data provide valuable insights into key parameters that may constrain gold mineralization, while also shedding light on the petrogenesis and physicochemical conditions of the Laoshan granite.

2. Geological Setting and Samples

The Jiaodong Peninsula is situated to the east of the Tanlu fault zone in the eastern part of the NCC as shown in Figure 1. The NCC, which is one of the largest cratons in East Asia, is made up of eastern and western blocks that were assembled at 1.85 Ga along the Trans-North China Orogen [13,14]. Subsequently, the NCC remained stable

for a considerable period with minimal deformation, metamorphism, and magmatism until the Early Mesozoic. However, the deep continental subduction of the Yangtze Block relative to the NCC initiated the destruction of the craton [15,16], which climaxed in the Early Cretaceous under the subduction of the Paleo-Pacific plate [8,17–21]). During the Mesozoic, the NCC was significantly influenced by multiple tectonic processes, leading to the extensive thinning of the lithospheric mantle (>80 km) and strong interactions between the crust and mantle [20,22–25], resulting in the formation of a large number of polymetallic deposits. Consequently, numerous polymetallic deposits were formed, and the Jiaodong gold province is a typical example of this tectonic setting (Figure 1).

The Jiaodong Peninsula is comprised of three main geological regions: the Jiaobei terrane, the Jiaolai Basin, and the Sulu orogenic belt (Figure 1B). A Precambrian basement and Jurassic to Early Cretaceous granites constitute the main lithology of the Jiaobei terrane (Figure 1B). The Precambrian basement is made up of the Neoproterozoic Jiaodong Complex (inclu: metamorphosed volcanic-sedimentary rocks and Archean tonalite–trondhjemite–granodiorite), Paleoproterozoic Jingshan and Fenzishan groups, and the Neoproterozoic Penglai group (meta-sedimentary rock series) [4]. The Jiaolai continental basin was formed in the Cretaceous period and is situated at the boundary between the Sulu orogen and Jiaobei terrane. This basin is mainly composed of volcanic-sedimentary rocks (Figure 1B). The Sulu orogen can be further divided into the Jiaonan terrane in the south and Weihai terrane in the northeast (Figure 1B), which are mainly composed of ultrahigh-pressure metamorphic rock series [4]. Faults are mainly distributed in the NE–NNE-striking of the Jiaodong Peninsula, with NNE-striking faults playing a significant role as the main ore-controlling structures (Figure 1B).

The Mesozoic granites are mainly distributed in the Jiaobei terrane and the Sulu orogen (Figure 1B), panning two periods: the Middle Jurassic and Early Cretaceous [4]. The Middle Jurassic granites (~160 Ma) are mainly composed of Linglong, Luanjiahe, Kunyushan, and Wendeng plutons (Figure 1B) (hereafter collectively referred to as the Linglong suite), which have similar mineral compositions and geochemical characteristics [26]. The Early Cretaceous granites are classified into Guojialing (132–125 Ma), Weideshan (125–110 Ma), and Laoshan (125–109 Ma) suites based on their formation age, mineral assemblage, and geochemical information [26,27]. Over 200 gold deposits have been discovered in the Jiaodong Peninsula, with most of them hosted in granites (77% hosted in the Linglong type, 10% in the Guojialing type [4]), and the formation time of the Jiaodong gold deposits are concentrated around ~120 Ma [1,3–7]. These magmatic rocks are closely related to the Jiaodong gold deposit, both temporally and spatially. The gold deposits are mainly found in magmatic rocks and are distributed along NNE-striking faults (Figure 1B).

The Laoshan-type granites are mainly distributed in the eastern and southern Jiaodong Peninsula. There is no direct spatial distribution relationship with gold mineralization and non-ferrous metal mineralization. In this study, the Laoshan granite is classified as part of the Xiaopinglan unit, which is a medium- to fine-grained alkali feldspar granite (labelled as 21LS01 samples herein; location: N 36°15.3'; E 120°27.8') (Figure 2B–D). The alkali feldspar granite primarily contains alkali feldspar (50–60%), quartz (25–30%), plagioclase (5–10%), and biotite (~1%), and zircon and apatite as the accessory phases (Figure 2B–D).

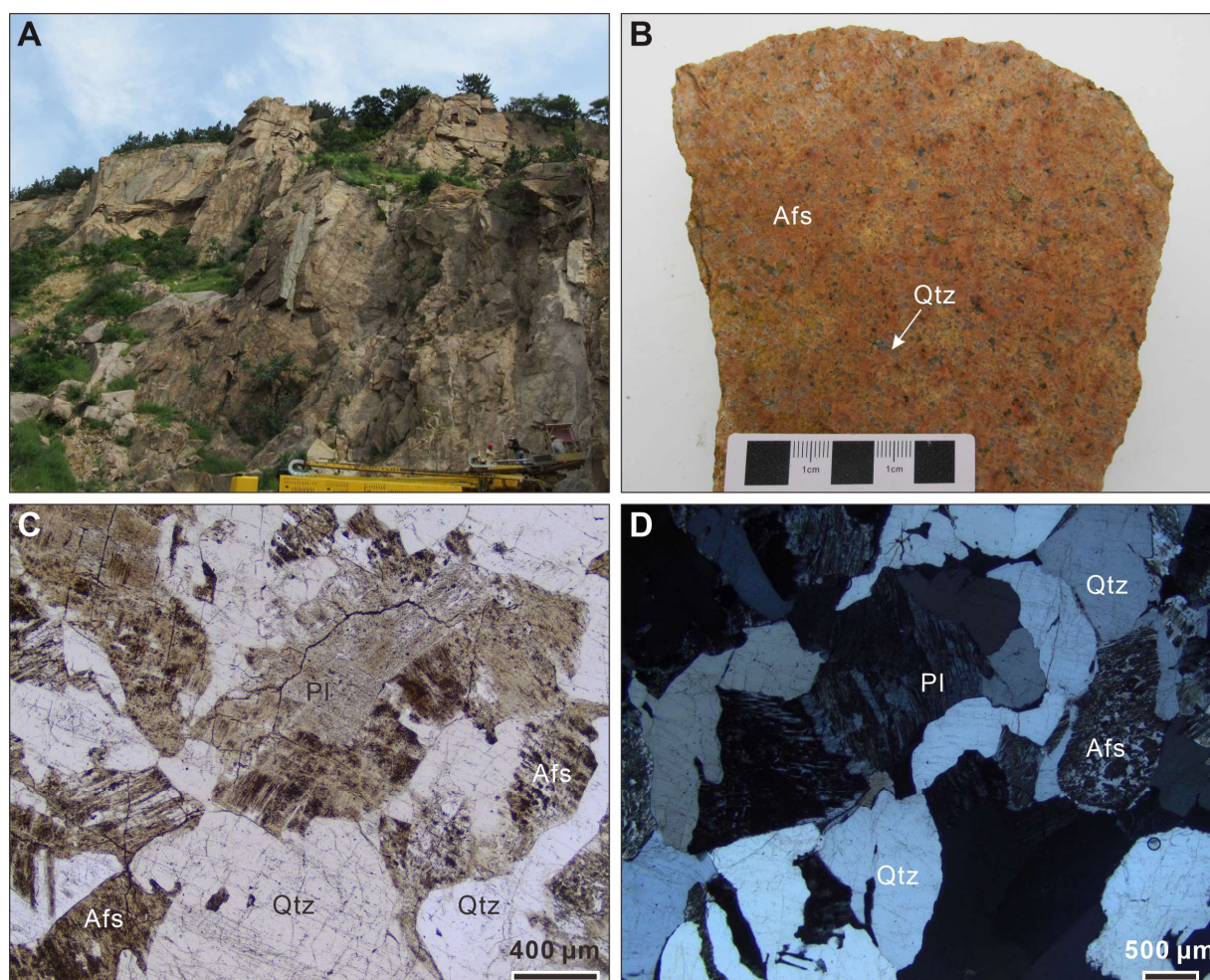


Figure 2. Representative photomicrographs of the Laoshan suite from the Jiaodong Peninsula ((A). Field photo; (B). Hand specimen photo; (C). Plane-polarized photo; (D). Cross-polarized photo). Afs = Alkali feldspar; PI = Plagioclase; Qtz = Quartz.

3. Analytical Methods

3.1. Zircon U–Pb Dating and Trace Elements

The zircon grains of the Laoshan granites (fresh and unaltered) were separated through traditional magnetic and heavy liquid techniques and manually selected under a binocular microscope, which was completed by Guangzhou Tuoyan Analytical Technology Co., Ltd. (Guangzhou, China). The selected zircons were carefully examined using transmitted, reflected light, and cathodoluminescence (CL) images to analyze the internal texture of the zircons, avoiding cracks and inclusions during laser ablation. The U–Pb age and trace element analyses of zircon were completed using laser ablation inductively coupled plasma mass spectroscopy (LA–ICP–MS) (193 nm LA system and Agilent 7900 ICP–MS instrument) at the Institute of Geology, Chinese Academy of Geological Sciences (Beijing, China). The test parameters were as follows: the spot was 30 μm , the energy was 2 J/cm^2 , and the repetition rate was 5 Hz. The selection of standard samples was to use 91500 (1062.4 ± 7.7 Ma; $n = 34$) as the external standard and NIST 610 glass and SA01 (533.7 ± 5.3 Ma; $n = 17$) were used to calibrate the age and trace elements (the analysis included two 91500 standard samples and one SA01 standard sample at every 10 sample points). Typically, a gas blank of 20 s was collected, and a signal interval of 35–40 s was used for data processing, followed by deep fractionation correction using an exponential equation [28]. Isoplot (Version 3.0 [29]) was used to obtain the concordia and weighted diagrams. The common Pb was corrected following the method described by T. Andersen [30].

3.2. Whole-Rock Major and Trace Element Analyses

We conducted 10 major element (21LS-1-1~5, 21LSS-1-1~5) and 5 trace element (21LS-1-1~5) analyses on Laoshan granite samples in this study, all of which were completed at Guangzhou Tuoyan Analytical Technology Co., Ltd. The major elements of the whole rock were determined with the Primus II X-ray fluorescence spectrometer (XRF), burned in a muffle furnace at 1000 °C for 2 h and the ignition loss (LOI) was calculated after cooling. The whole-rock trace elements analysis was completed using the Semferri CAP RQ system. During the test, the accuracy of data results was monitored with OU-6, BCR-1, and GBPG-1 as standard samples, and the RSD of data results was better than 5%.

4. Results

4.1. Zircon U–Pb Ages and Trace Elements Composition

Zircon grains of Laoshan granite exhibit clear oscillatory zones, with a length of 100–300 μm and a width of 40–100 μm , and contain a few mineral inclusions (Figure 3A). The REEs composition in the zircons reveal notable positive Ce anomalies (ranging from 3.49 to 1448.73) (Figure 3B), along with high Th/U ratios (0.54–2.77), indicating that these are magmatic zircons [31,32]. Twenty-nine analyses of zircon from the alkali feldspar granite 21LS01 gave $^{206}\text{Pb}/^{238}\text{U}$ ages of 121 ± 3 Ma to 113 ± 4 Ma (Supplementary Table S1), yielding a weighted mean $^{206}\text{Pb}/^{238}\text{U}$ age of 118 ± 1 Ma (MSWD = 0.31) (Figure 3C,D). This age is interpreted as the emplacement age of the alkali feldspar granite. Zircon trace element data are presented in Figure 4, showing significant negative correlations between zircon Ce/Yb, Sc/Yb, ΔFMQ , Th/U, and Gd/Yb and Hf elements, while U/Yb shows a positive correlation (Figure 4).

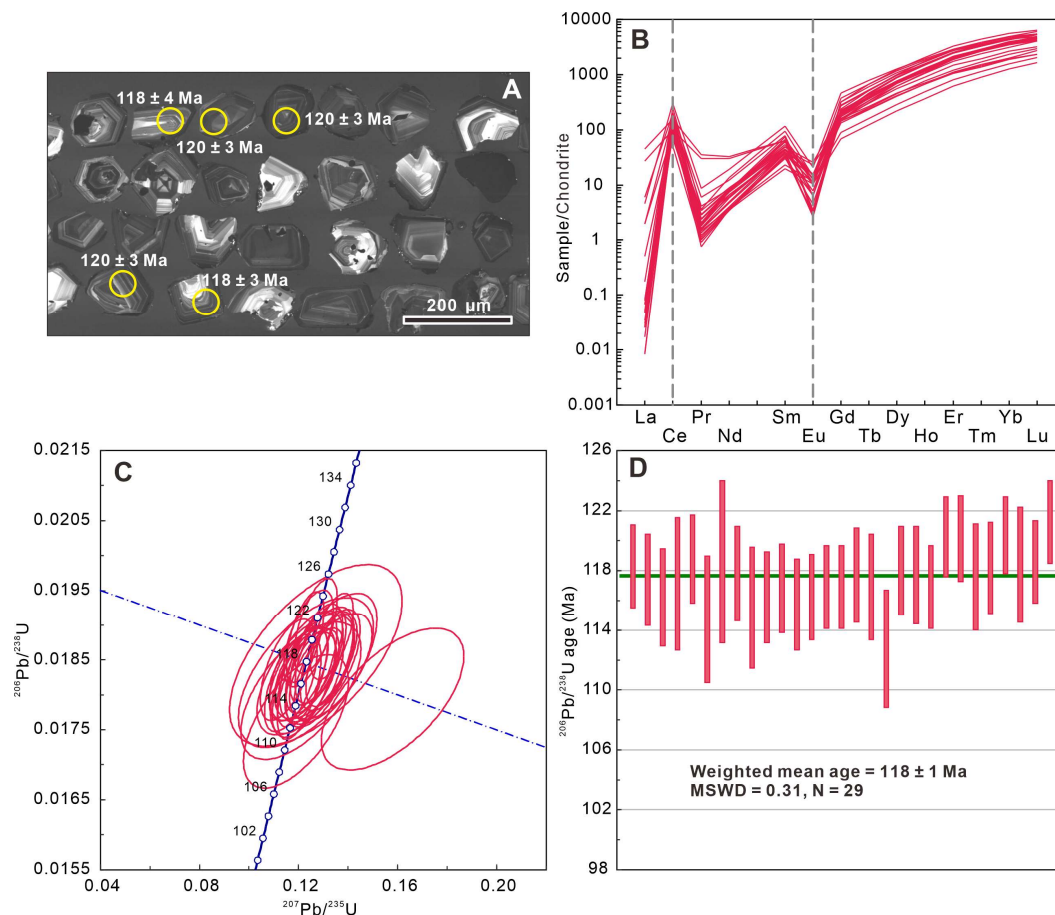


Figure 3. (A). Representative CL images; (B). Chondrite-normalized REE patterns; (C). Zircon U–Pb concordia diagram. (D). Weighted mean $^{206}\text{Pb}/^{238}\text{U}$ age diagram.

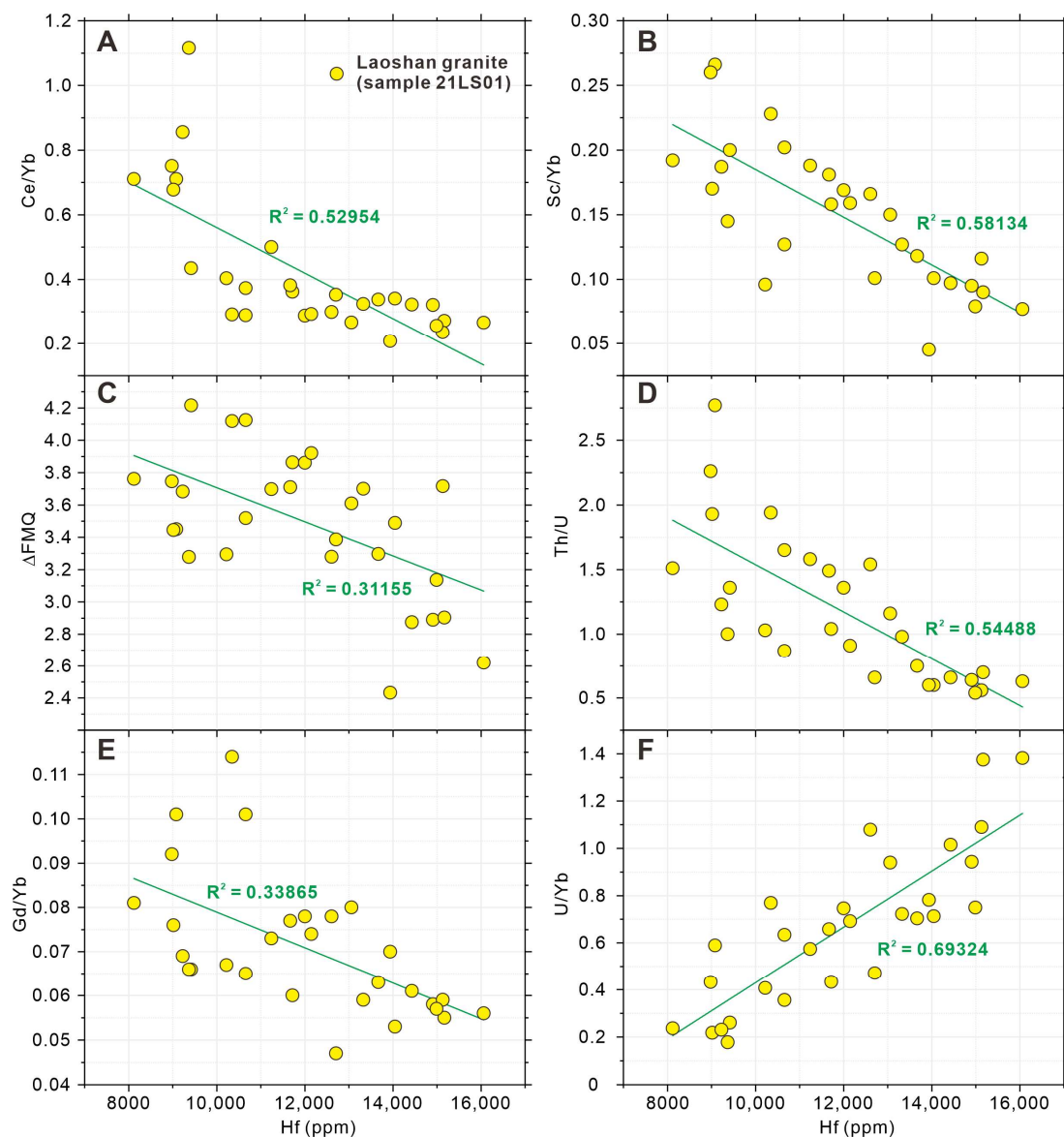


Figure 4. Ce/Yb (A), Sc/Yb (B), Δ FMQ (C), Th/U (D), Gd/Yb (E), and U/Yb (F) vs. Hf plots of zircons from the Laoshan suite.

4.2. Whole-Rock Major and Trace Element Geochemistry

The whole-rock major and trace element compositions of the Laoshan granite are listed in Supplementary Table S2. We also systematically collected the geochemical data of the Mesozoic igneous rock in the whole Jiaodong Peninsula, which are listed in Figures 5–7 together with the Laoshan granite. The Laoshan granite exhibits high contents of SiO_2 (76.03–80.28 wt.%), Na_2O (3.51–4.01 wt.%), and K_2O (3.94–4.61 wt.%), falling within the granite range and belonging to the subalkaline series in the SiO_2 vs. $\text{Na}_2\text{O} + \text{K}_2\text{O}$ diagram (Figure 5A). Some previous data fall within the quartz monzonite range of the alkaline series (Figure 5A). They belong to the high-K calc-alkaline series in the plot of SiO_2 vs. K_2O (Figure 5B). All samples in this study fall within the peraluminous range in the A/CNK-ANK diagram, while previous data fall within the metaluminous to peraluminous range (Figure 5C). In the Harker diagrams, the correlation between SiO_2 vs. Al_2O_3 , CaO, MgO, P_2O_5 , TFe_2O_3 , and TiO_2 (Figure 6) is significant (especially adding published data), indicating the crystallization differentiation of minerals.

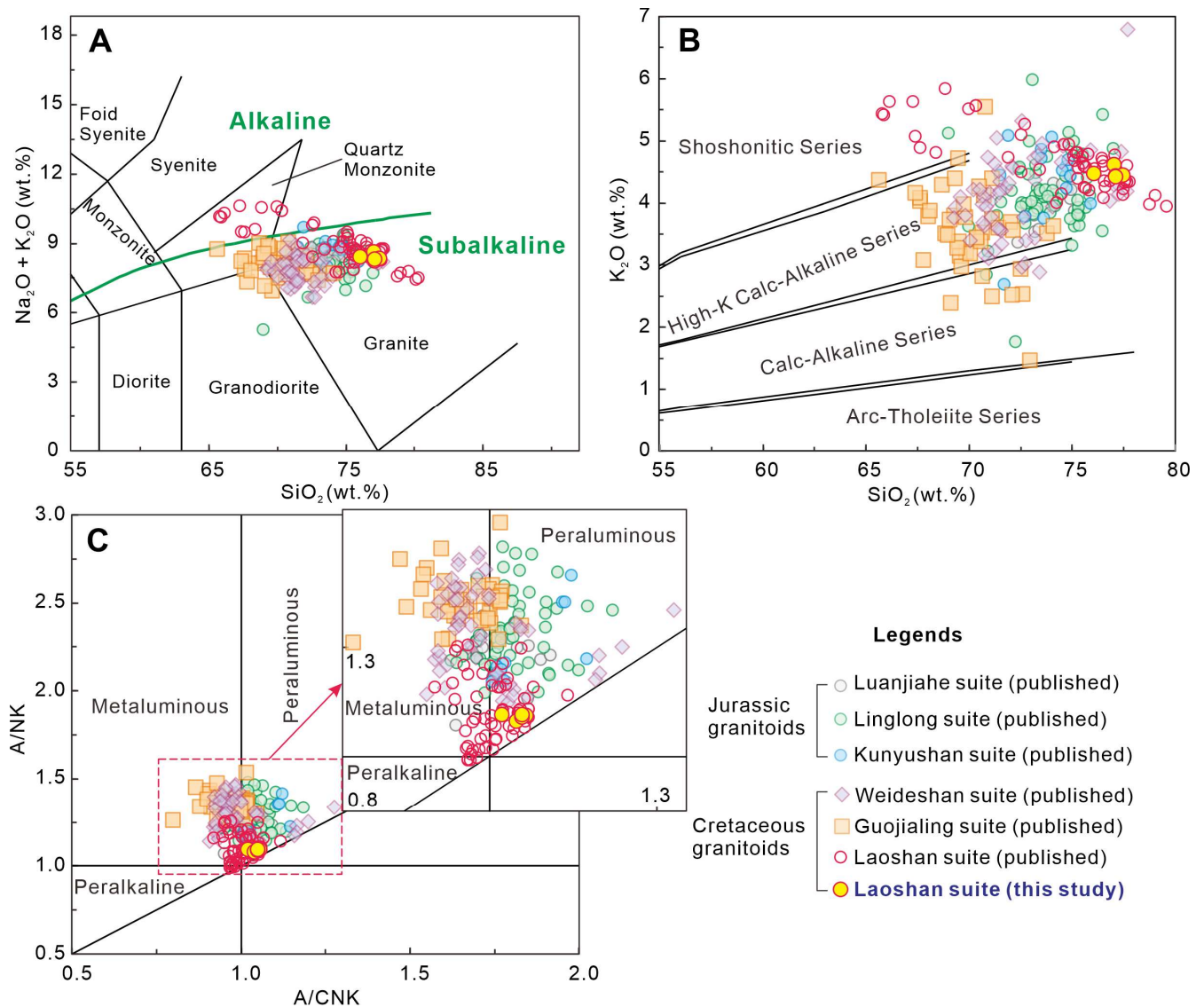


Figure 5. Whole-rock geochemistry plots for the Jiaodong Peninsula Mesozoic granitoids. (A). Total alkalis ($\text{Na}_2\text{O} + \text{K}_2\text{O}$) vs. silica (SiO_2) [33]; (B). K_2O vs. SiO_2 [34]; (C). A/NK vs. A/CNK [35]. Note: A/CNK = molar ratio of $\text{Al}_2\text{O}_3/(\text{CaO} + \text{Na}_2\text{O} + \text{K}_2\text{O})$; A/NK = molar ratio of $\text{Al}_2\text{O}_3/(\text{Na}_2\text{O} + \text{K}_2\text{O})$. Published data are from this study and [26,27,36–46].

In the REEs composition, the Laoshan granite has obvious characteristics of being enriched in LREE and depleted in HREE ($\text{La}_N/\text{Yb}_N = 6.30\text{--}8.09$; $\text{LREE}/\text{HREE} = 5.94\text{--}6.90$) (Figure 7G). The negative Eu anomaly is significant ($\text{Eu}/\text{Eu}^* = 0.06\text{--}0.08$), with a clear V-shaped pattern, and the published data also exhibit this characteristic (Figure 7G). In the trace element spider diagrams, all samples are enriched in large-ion lithophile elements (LILEs, e.g., Rb and Pb) and depleted in high-field-strength elements (HFSEs, e.g., Nb, Ta, and Ti) and P (Figure 7H). The Linglong, Guojialing, and Weideshan suites also exhibit such characteristics (Figure 7B,D,F).

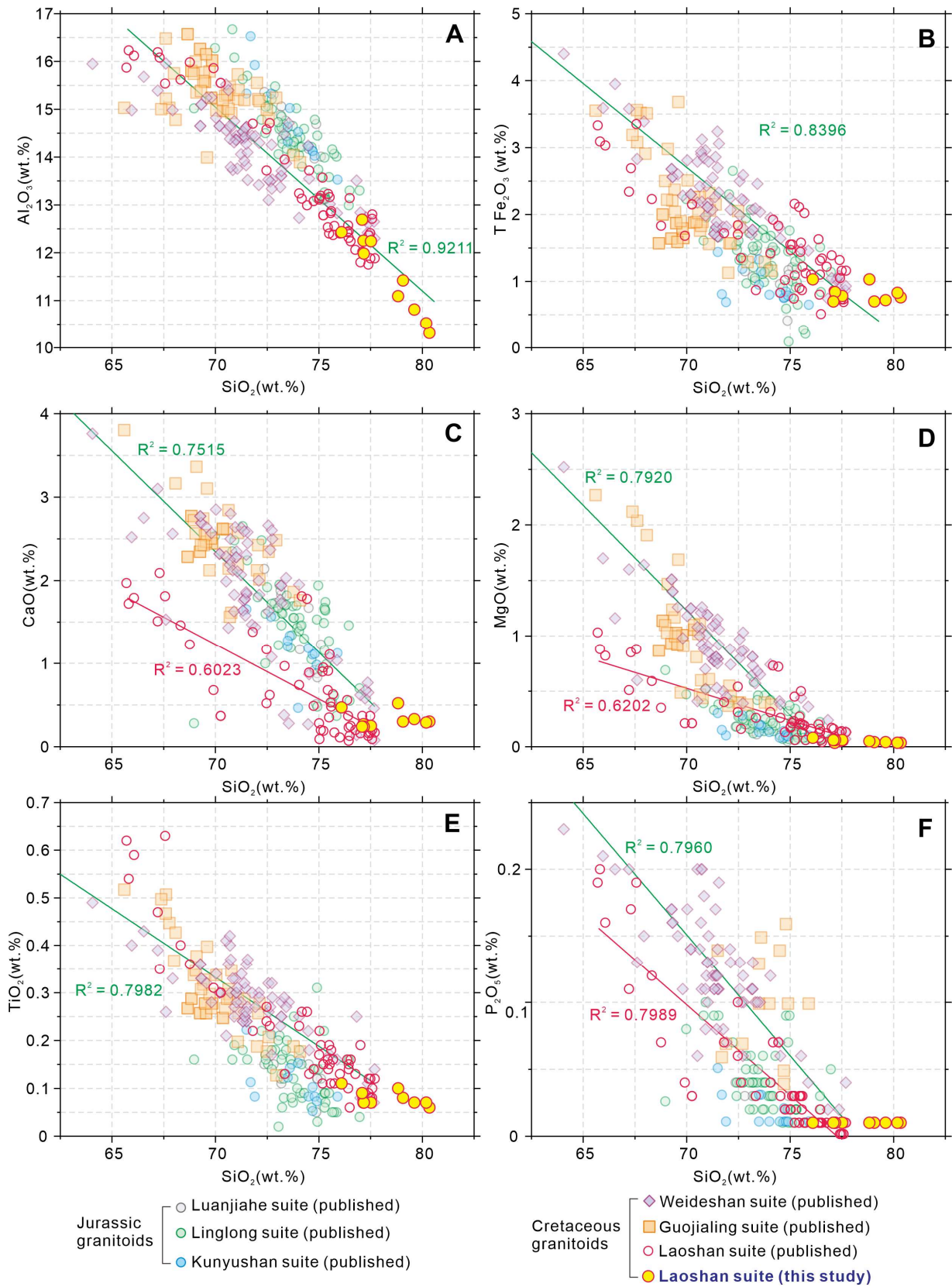


Figure 6. Al₂O₃ (A), TFe₂O₃ (B), CaO (C), MgO (D), TiO₂ (E), and P₂O₅ (F) vs. SiO₂ plots of Mesozoic granitoids from the Jiaodong Peninsula. The published data are the same as in Figure 5.

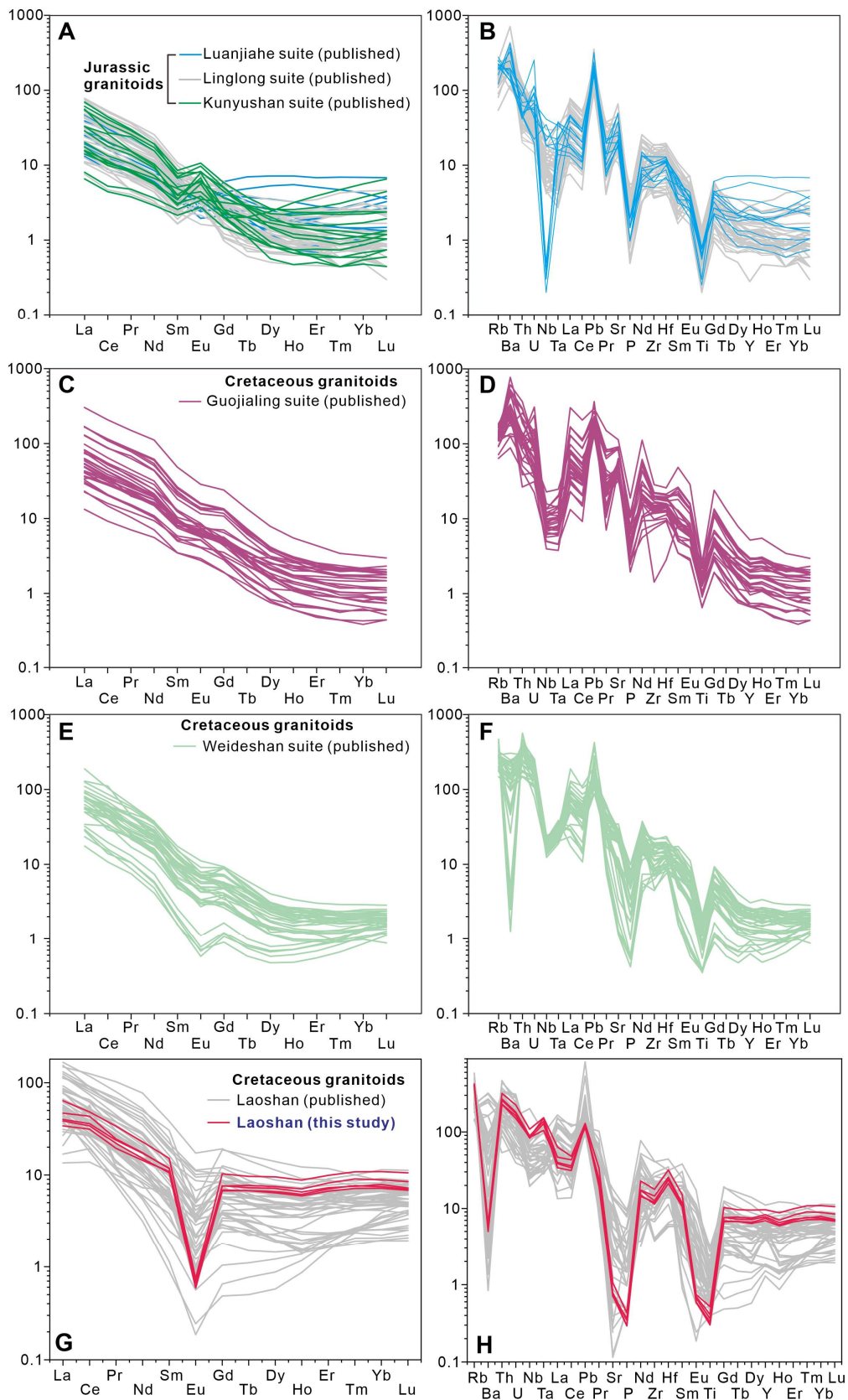


Figure 7. Chondrite-normalized REE patterns (A,C,E,G) and primitive mantle-normalized trace element variation diagrams (B,D,F,H) for the Jiaodong Peninsula Mesozoic granitoids. Normalizing values are from McDonough and Sun [47]. The published data are the same as in Figure 5.

5. Discussion

5.1. Magma Types, Sources, and Petrogenesis

Adakitic geochemical features are widely regarded as important for the formation of large deposits (e.g., porphyry Cu deposits [48–52]). The Linglong, Guojialing, and Weideshan suites have highly variable Sr/Y (35.54–136.50) and La/Yb (1.43–176.43) ratios, and low Y (3.26–11.20 ppm) and Yb (0.33–0.97 ppm) contents [26,36–39,42,43], indicating an adakitic affinity. Furthermore, in the Sr/Y vs. Y and (La/Yb)_N vs. Yb_N discrimination diagrams, these samples fall in the adakite field (Figure 8).

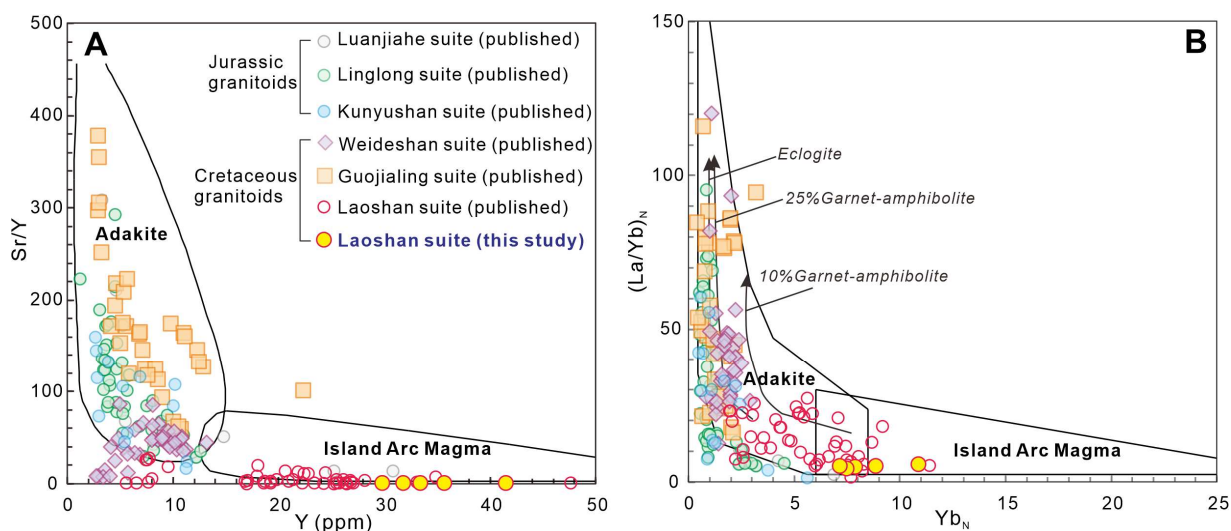


Figure 8. (A). Sr/Y vs. Y (after Martin [53]; Defant and Drummond [54]); (B). (La/Yb)_N vs. Yb_N (after Martin [55]; Drummond et al. [56]; Martin et al. [57]). The published data are the same as in Figure 5.

In contrast, the Laoshan suite has low Sr/Y (0.09–27.78) and La/Yb (2.58–40.27) ratios, and low Y (5.56–41.50 ppm) and Yb (0.85–4.80 ppm) contents (this study and [40,41,44,46]), indicating a normal-arc geochemical character (Figure 8).

5.1.1. Adakite-like Rocks: Linglong, Guojialing, and Weideshan Suites

The Linglong, Guojialing, and Weideshan suites exhibit high SiO₂ (65.60–77.69 wt.%), and low TFe₂O₃ (0.09–3.70 wt.%) and MgO (0.05–2.28 wt.%) contents [26,36,38,39,42,43]. These rocks are depleted in Nb, Ta, Ti, and P (Figure 7), indicating that they may have originated from the partial melting of crustal material [58,59]. The characteristic trace element ratios suggest that these rocks are primarily crustal-derived. Firstly, the average Zr/Hf (33.7) and Nb/Ta (13.0) ratios are significantly lower than those of the primitive mantle values (37 and 17.8, respectively [47]), but closer to the values of the average crustal values (33 and 11.4, respectively [60,61]). Secondly, the average Ce/Pb (3.3) and Nb/U (5.0) ratios reflect a continental crustal source (4 and 10, respectively [62]). Thirdly, the low compatible element (e.g., Co and Ni) contents indicate a lower crustal source [63]. In addition, the granites fall within the thickened lower crustal range in SiO₂ (wt%) versus MgO (wt%), Mg#, and Ni diagrams (Figure 9). Considering the regional geological setting, the Jiaodong Peninsula was in a subduction environment of the Paleo-Pacific Plate during the Middle Jurassic–Early Cretaceous. Therefore, the Linglong, Guojialing, and Weideshan adakitic magmatic rocks are products of the partial melting of the thickened lower crust. However, the variable Mg# value (10–59) suggests that there may also be mixing of mantle components in the magma source. The Linglong granite is characterized by a gneissic structure, no enclaves, and a Mg# < 40 [36,38,39,42]. It contains xenoliths of Precambrian strata, indicating that it originated from the remelting of ancient crustal materials. The Sr–Nd isotope diagram shows that the Linglong granite is closer to the crust and also supports

crustal sources (Figure 10A). As for the Early Cretaceous Guojialing and Weideshan granites, a large number of mafic enclaves were developed [4], and their Sr–Nd isotopic composition was also close to the mantle evolution trend, indicating a significant involvement of mantle-derived materials (Figure 10A). The adakitic rocks formed by these granites have a lower zirconium saturation temperature than the Laoshan granite (Figure 10B).

The La vs. La/Yb and La/Sm diagrams indicate that these granites were formed by partial melting of crustal materials (Figure 11A,B). On the Sr/Nd vs. Th/Yb and Nb/Y vs. Ba diagrams (Figure 11C,D), the Weideshan suite shows a distinct trend from other granites, suggesting a melt-related enrichment feature, while the Linglong and Guojialing suites are fluid-related. This indicates that the mafic magma during the formation of the Weideshan granite may be attributed to the partial melting of a mantle wedge that had been metasomatized by subduction slab-derived melts rather than slab-derived hydrous fluids (e.g., Ji et al. [64]).

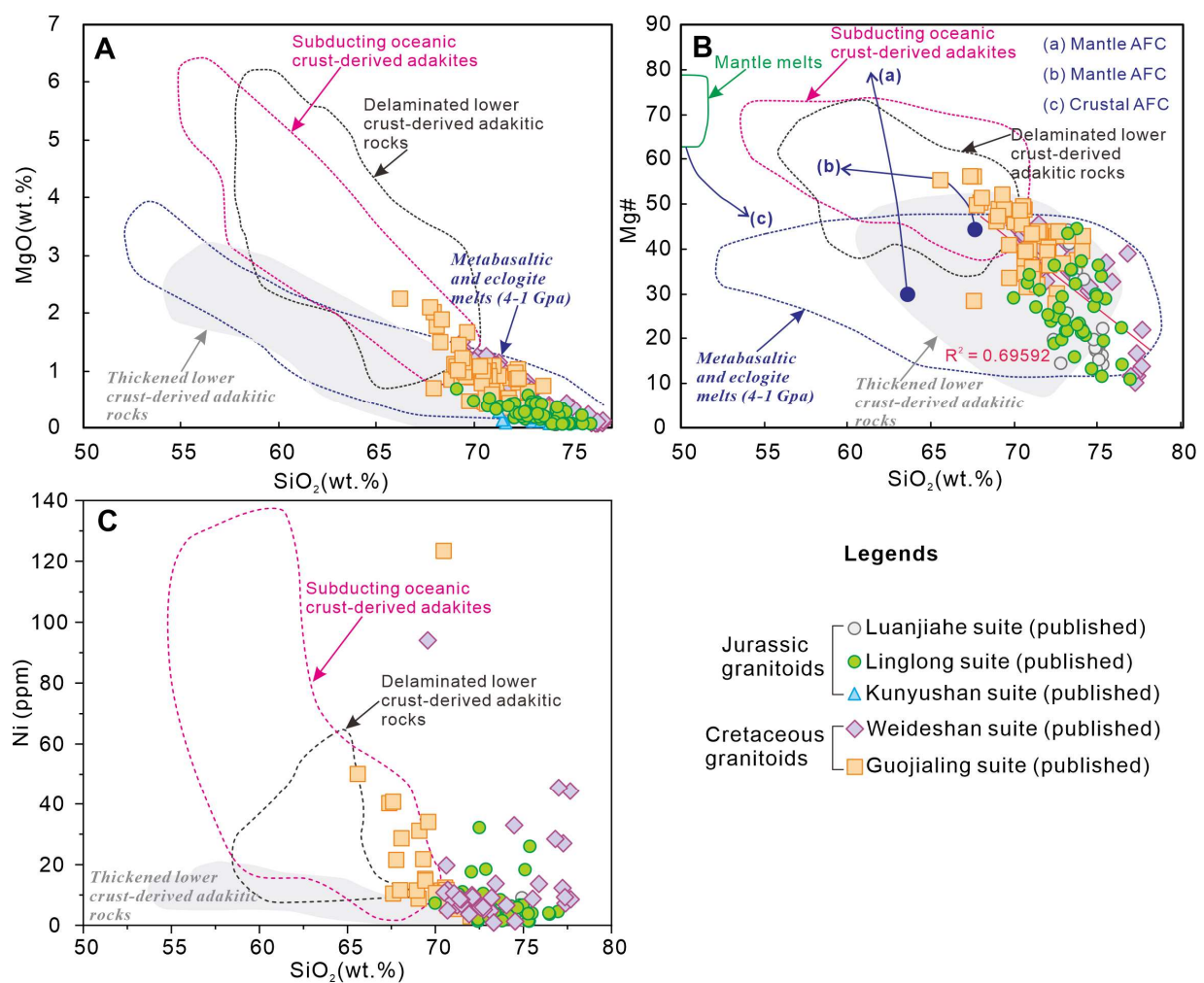


Figure 9. Plots of MgO (A), Mg# (B), and Ni (C) vs. SiO₂ for the Mesozoic adakitic rocks in the Jiaodong Peninsula. The published data are the same as in Figure 5. Note: the subducting oceanic crust-derived adakites are from Defant and Drummond [54], Stern and Kilian [65], Martin [66], Smithies [67], and Defant et al. [68]; the thickened lower crust-derived adakitic rocks are from Atherton and Petford [69], Petford and Atherton [70], Muir et al. [71], and Smithies [67]; the delaminated lower crust-derived adakitic rocks are from Xu et al. [72].

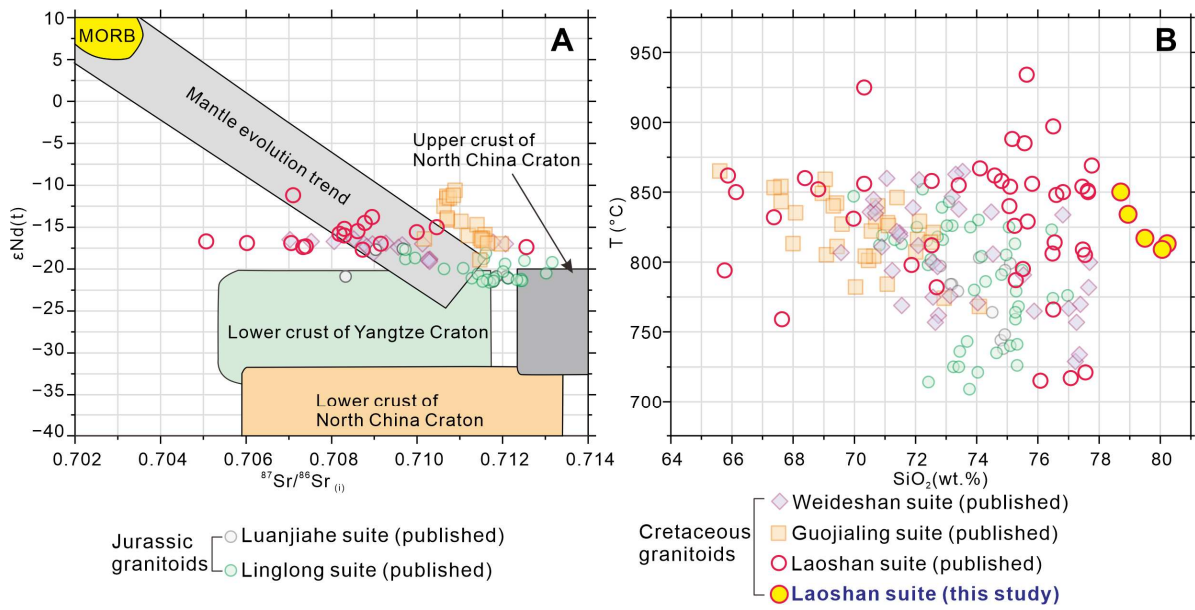


Figure 10. Plots of $\epsilon Nd(t)$ vs. $(^{87}Sr/^{86}Sr)_i$ ratio (A) and SiO_2 vs. T-Zr (B) diagrams for the granites from the Jiaodong Peninsula. The published data are the same as in Figure 5.

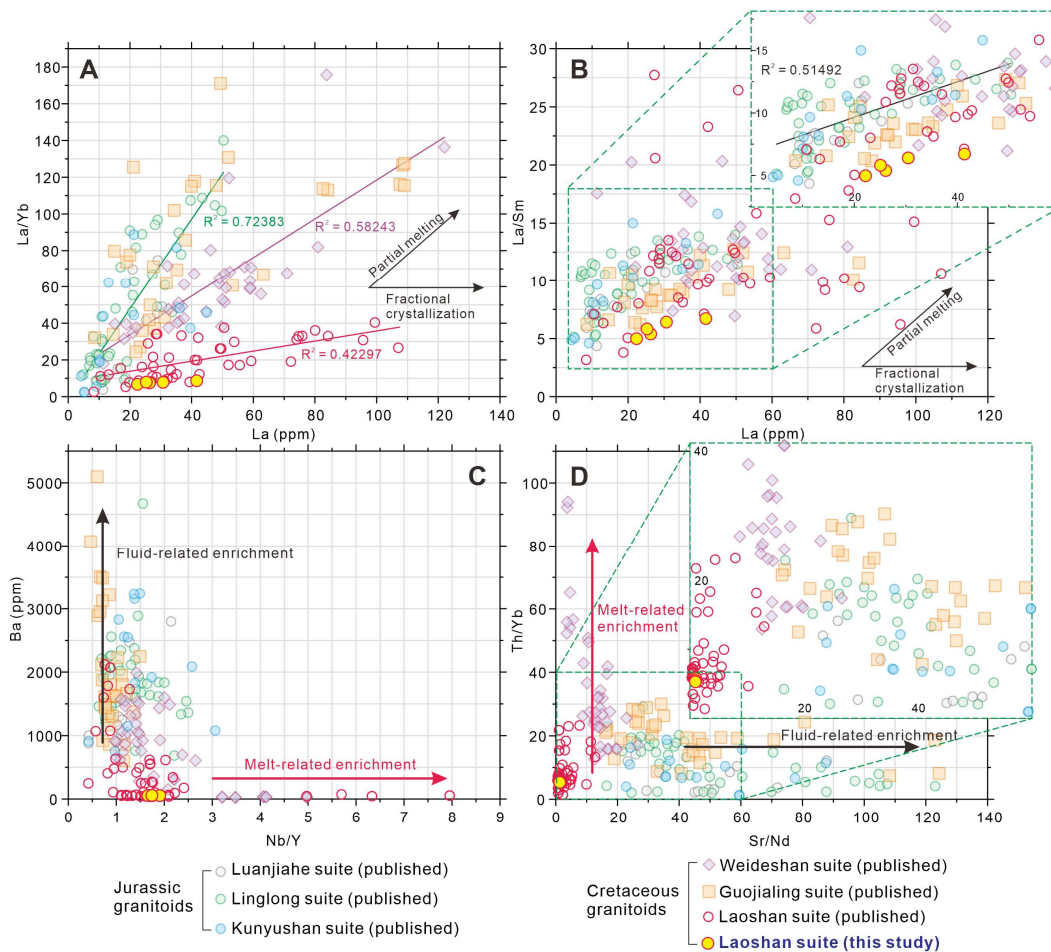


Figure 11. Plots of (A) La vs. La/Yb, (B) La vs. La/Sm, (C) Sr/Nd vs. Th/Yb [73], and (D) Nb/Y vs. Ba [74] for the Mesozoic granites from Jiaodong Peninsula. The published data are the same as in Figure 5.

5.1.2. A-Type Granite: Laoshan Suites

As previously mentioned, the Laoshan suite exhibits low Sr/Y and La/Yb ratios, as well as low Y and Yb contents, which are indicative of a typical normal-arc magma. These igneous rocks have a high SiO₂ content (65.76–80.28 wt%), low Mg# value (6–44) and compatible element (e.g., Co and Ni) content, and an aluminum deficiency (A/CNK = 0.92–1.12, lack of Al-rich minerals) (this study and [40,41,44,46]). This set of characteristics rules out the possibility of M- and S-type granites [75]. Additionally, these granites have high total alkalis (7.45–10.63 wt%), Zr (39.3–437.5 ppm), Ce (23.12–209.28 ppm), Nb (12.8–132.0 ppm), and Y (5.56–41.50 ppm) contents, and low CaO (0.07–2.09 wt%) and MgO (0.03–1.03 wt%) contents. They are also characterized by high TFe₂O₃/MgO (3.2–33.5) and Ga/Al (0.6–4.0) ratios, high varying zircon saturation temperatures (715–934 °C [76]), and remarkable negative Eu (Eu/Eu* = 0.05–0.80) anomalies (this study and [40,41,44,46]). These features strongly suggest that the Laoshan suite has the characteristics of A-type granite (e.g., Li et al. [77]). The data points in the 10000 Ga/Al vs. K₂O/MgO, Nb, (Na₂O + K₂O)/CaO, and TFe₂O₃/MgO plots also fall within the range of A-type granite (Figure 12A–D) and belong to A1-type granite (Figure 12E,F). Furthermore, these granites all have lower Ba and Sr contents, which are typical of low Ba–Sr granites (Figure 13).

The A-type granites discussed in this study are characterized by high SiO₂ and low MgO contents, and are depleted in Nb, Ta, P, and Ti, while enriched in Rb and Pb. These features suggest that their formation can be attributed to partial melting of the crust [58,59]. These rocks also exhibit low average ratios of Nb/Ta (15.8), Zr/Hf (28.6), Ce/Pb (3.5), Nb/U (13.8), Rb/Sr (13.7), Ti/Zr (8.6), and Ti/Y (67.1) (this study and [40,41,44,46]), further supporting a lower crustal source [47,60–62,78–80]. However, the Laoshan suite appears to be located in or near the mantle channel on the ⁸⁷Sr/⁸⁶Sr vs. εNd(t) diagram (Figure 10A), suggesting possible mixing with mantle material. Moreover, similar to the Weideshan suite, the Laoshan granite exhibits a trend of melt-related enrichment in Sr/Nd vs. Th/Yb and Nb/Y vs. Ba diagrams (Figure 11C,D), indicating that it is also a result of partial melting of mantle wedges derived from subduction plate-derived melt metasomatism.

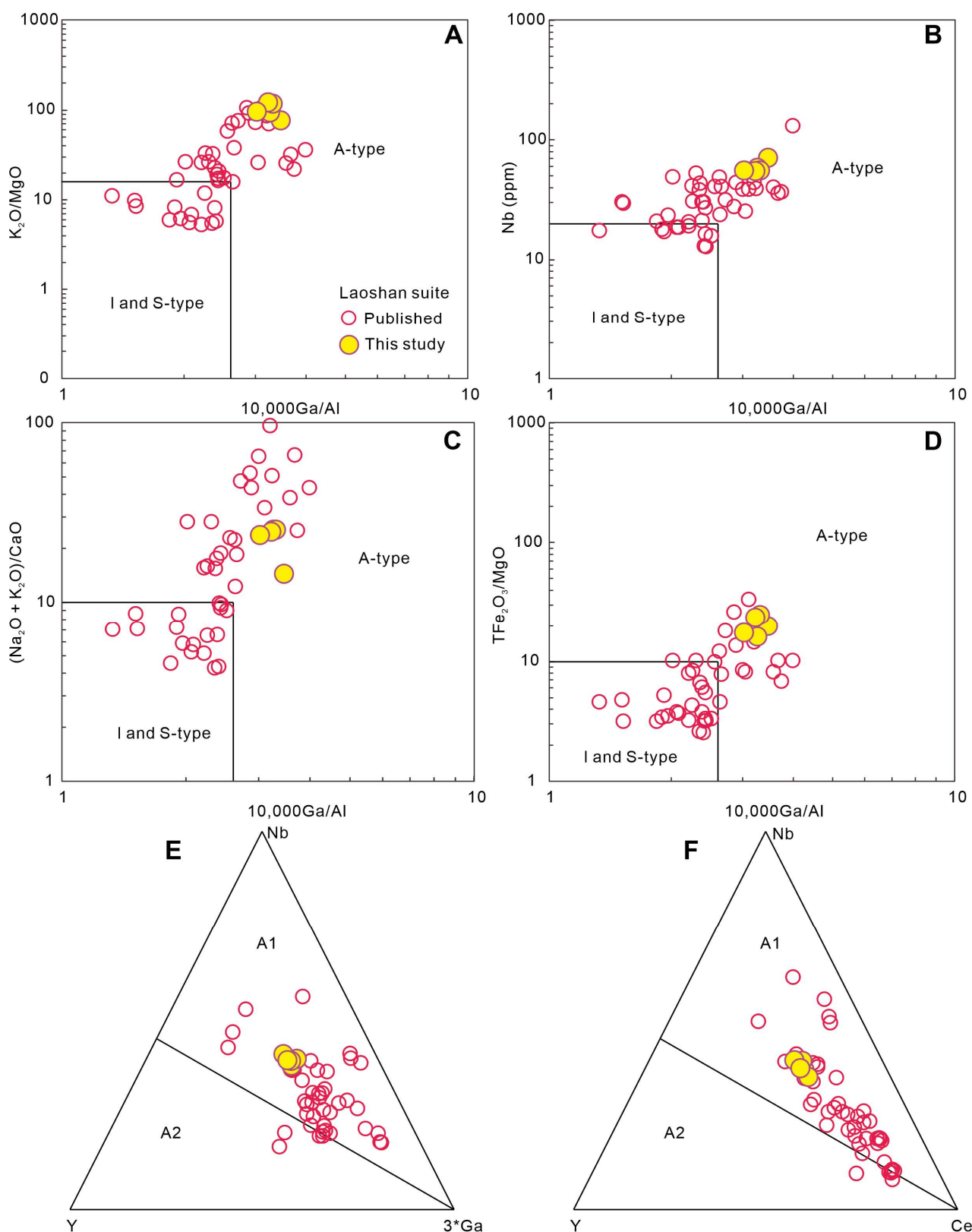


Figure 12. Plots of K_2O/MgO (A), Nb (B), $(Na_2O + K_2O)/CaO$ (C), and TFe_2O_3/MgO (D) vs. $10000 Ga/Al$ (Whalen et al. [81]), Nb–Y–3*Ga (E), and Nb–Y–Ce (F) (Eby [82]) discrimination diagrams for the Laoshan suite.

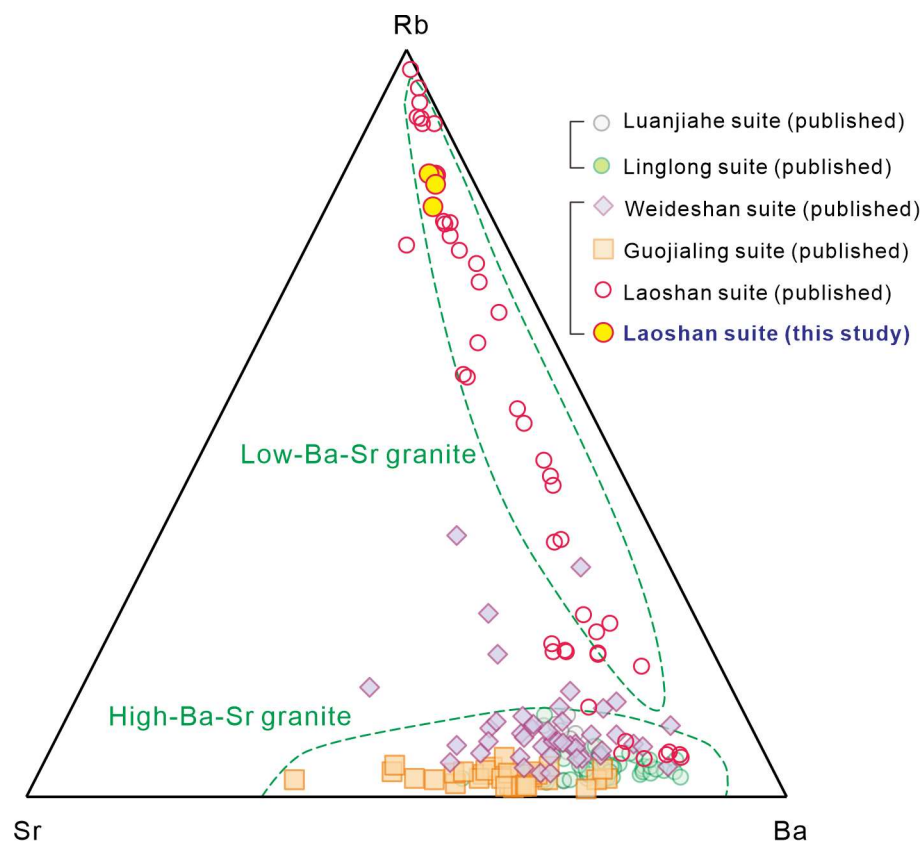


Figure 13. Sr–Rb–Ba plot for the Laoshan suite in the Jiaodong Peninsula (Qian et al. [83]).

5.2. An oxidized Low Ba–Sr Granite

Previous studies on porphyry mineralization systems, particularly Cu–Mo mineralization [52,84], have indicated that the oxidation state of magma is closely related to mineralization [52,84]. Under high oxygen fugacity conditions, sulfur exists in the form of sulfates in magma (S^{6+} : HSO_4^-/SO_4^{2-}), which can significantly inhibit the early saturation and decomposition of sulfides (S^{2-}), as well as the consequent loss of chalcophile elements in the deeper crust [85,86]. Additionally, the migration of Au in hydrothermal fluids is mainly related to sulfur complexes [87], meaning that high oxygen fugacity in the magma source area also inhibits the early precipitation of Au. To calculate the Laoshan granite, we used the latest method provided by Loucks et al. [88], which avoids the disadvantage of the prevailing zircon oxybarometries. The analysis uncertainty of La is large in these methods, because minerals such as titanate, plagioclase, or apatite are fractionated before zircon [89,90]. The pressure data used in the specific calculation process are based on the average of EPMA data of amphibole and biotite from Dong et al. [91]. The results show that the ΔFMQ values of the Laoshan suite are 2.43–4.22, which are significantly higher than those of the Weideshan and pre-mineralization Linglong suite (Figure 14) [11,91]. Furthermore, the Ti-saturation temperature is also significantly higher than that of the Weideshan and Linglong suites, which is also consistent with the basic characteristics of A-type granite (Figure 14A) [82]. This studied Laoshan granite was formed at ~118 Ma, and the entire Laoshan suite was formed over a large time span of 125–108 Ma [44,92,93]. The location is distant from the known gold deposits (Figure 1), and it is considered to be a post-mineralization granite. Therefore, the Laoshan suite belongs to a low Ba–Sr granite with high oxygen fugacity after mineralization.

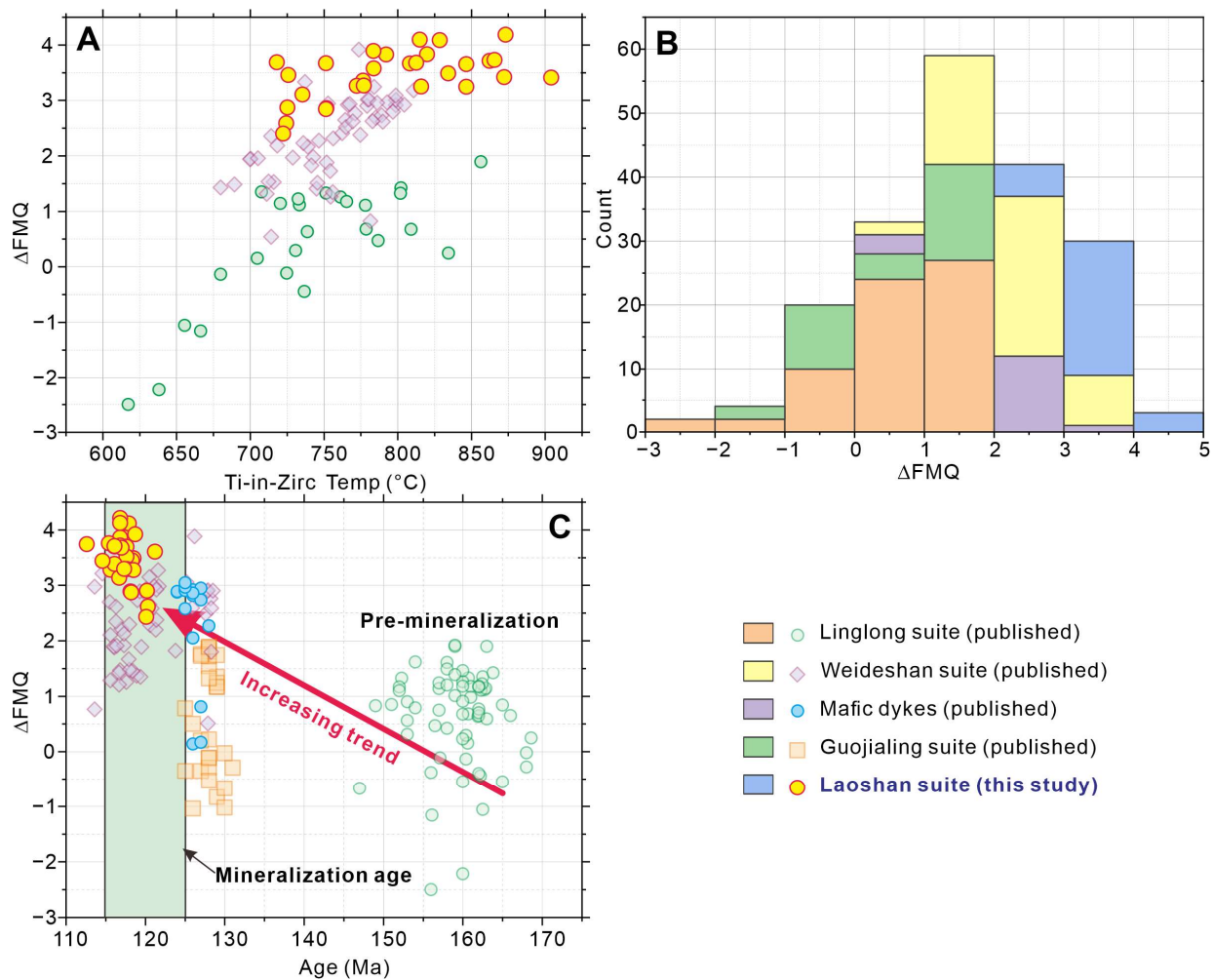


Figure 14. (A). T-Ti ($^{\circ}\text{C}$) (Ti-saturation temperature) vs. ΔFMQ ; (B). ΔFMQ histogram; (C). Age (Ma) vs. ΔFMQ . Ti-saturation temperature and ΔFMQ values are calculated from zircon trace elements (Table S3).

5.3. Tectonic Setting and Gold Mineralization Implication

The tectonic setting of the eastern NCC has been extensively studied, and a consensus has been reached that it is mainly influenced by the subduction of the Paleo-Pacific Plate [52,94–96]. The studied suites of Linglong, Guojialing, and Weideshan, which are of Jurassic to Early Cretaceous age, all fall within the category of volcanic arc granites (VAG) in the tectonic discrimination diagrams (Figure 15). This suggests that they were formed in a subduction environment. On the other hand, the Laoshan granites in this study and published data fall within the range of post-collision and syn-collision (Figure 15), indicating that they were formed in an extensional environment. Therefore, the tectonic nature of the Jiaodong Peninsula shifted from compression to extension from the Jurassic to the Early Cretaceous, and gold mineralization occurred during this transition. Additionally, the geochemical characteristics of granitoids in Jiaodong have changed significantly from the Jurassic to Early Cretaceous: (i) The Linglong, Guojialing, and Weideshan suites exhibit geochemical properties of adakitic rocks (Figure 8), whereas the Laoshan suite is a typical A-type granite (Figure 12); (ii) The positive Eu anomaly of the Jurassic Linglong granite transformed into the negative Eu anomaly of the Early Cretaceous Laoshan granite in terms of REE composition (Figure 7); (iii) The Mesozoic granites of the Jiaodong Peninsula are all related to partial melting of thickened lower crustal material associated with oceanic crustal subduction. The Linglong suite has no mantle material admixture, while the Guojialing, Weideshan, and Laoshan suites have a large amount of mantle material mixing

(Figures 9 and 10) and petrographic development of a mafic microgranular enclave (MME) (e.g., Song et al., [2]); (iv) From the Jurassic to Early Cretaceous, the oxidation state of the magma source area changes and becomes gradually oxidized, with the highest ΔFMQ value for Laoshan granite (Figure 14); (v) From the Jurassic to the Cretaceous, the lithospheric mantle properties changed from enrichment to depletion [2].

The concentrated mineralization in the Jiaodong region occurred during the Early Cretaceous (120 ± 5 Ma; [3,5]), which corresponds to the period of transformation of tectonic setting and magma geochemistry mentioned above. The adakitic magma with high oxygen fugacity, medium negative Eu anomaly, extensional tectonic system, and mixed mantle material may have facilitated the formation of gold deposits. In the Jurassic Linglong granite, there are no MMEs or amphiboles, while in the Early Cretaceous granites, there are a large number of MMEs, amphiboles, and contemporaneous mafic dykes. This suggests the mixing of mantle materials may have contributed to magma oxidation and water enrichment (e.g., Dong et al. [91]). Therefore, we have established such a tectonic evolution model from the Jurassic to the Cretaceous: (a) During the Jurassic period, the ancient crustal materials were partially melted under the subduction of the Paleo-Pacific Plate, forming Linglong granite. In the region, it is common to find xenoliths containing strata in Linglong granite and displaying gneissic structures. Moreover, the Jurassic mafic dykes are almost not developed, which also suggests that the Linglong granite with low oxygen fugacity and low water content was formed by partial melting of the lower crust. This process may have promoted the saturation and accumulation of sulfides (which may also include gold) [91], causing the pre-enrichment of some key elements (e.g., sulfur) related to mineralization. (b) During the Cretaceous period, the subduction slab of the Paleo-Pacific Plate roll-back resulted in a significant upwelling of asthenosphere materials, making the tectonic nature change into extensional. The upwelling of mantle material and the mixing with a partially melted lower crust formed Early Cretaceous MME-rich granites. These crust–mantle magmas have high oxygen fugacity, carry a large amount of metal sulfides, and enrich at fault locations to form gold deposits. This suggests that the injection of mafic magma contributes to the increase in oxygen fugacity, which in turn leads to the enrichment of metal sulfides at fault locations, resulting in gold deposits. The current model provides valuable insights into the explosive and instantaneous mineralization of Jiaodong gold deposits, and also suggests that Jiaodong gold deposits may differ from traditional orogenic gold deposit categories [97]. In contrast, the formation of low Ba–Sr granites with higher oxidation levels, such as those in the Laoshan suite, was facilitated by the continued subduction of the Paleo-Pacific Plate. However, the lack of fault development in and around the Laoshan suite has prevented the formation of gold deposits. Additionally, the low Ba–Sr content may be attributed to less mantle material injection, which is one of the reasons for non-mineralization.

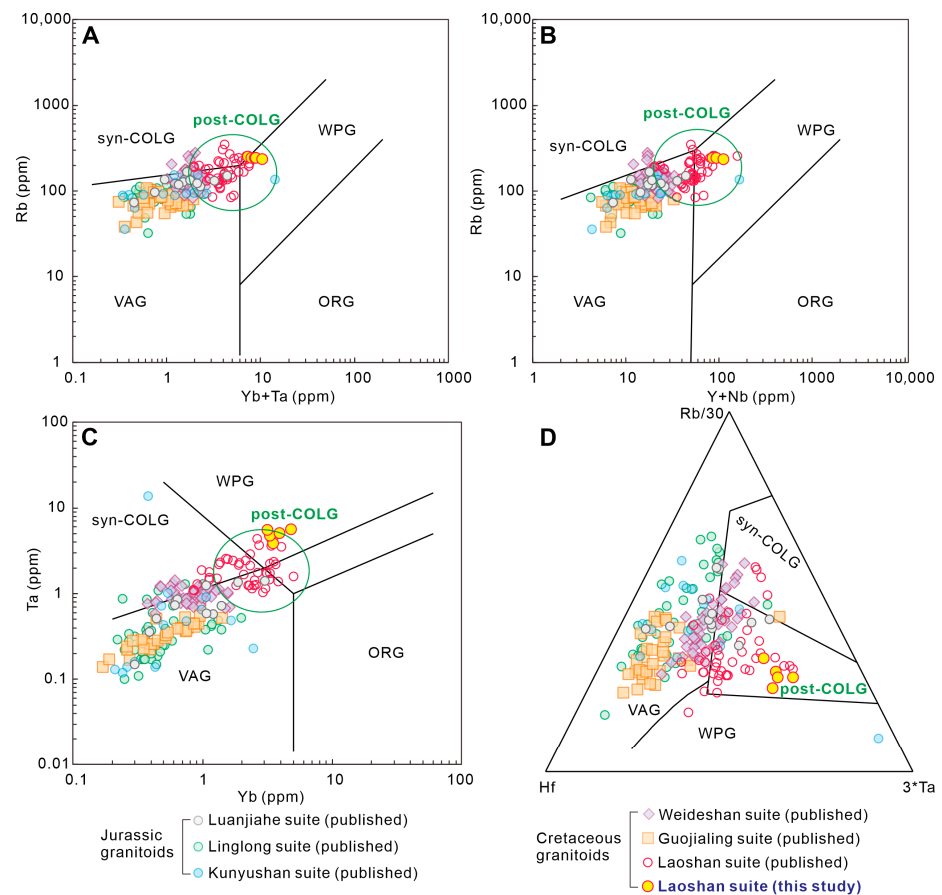


Figure 15. Tectonic discrimination diagrams for granitoids from the Jiaodong Peninsula. (A) Rb vs. (Yb + Ta) [98]; (B) Rb vs. (Y + Nb); (C) Ta vs. Yb [99]; (D) Rb/30-Hf-3*Ta [100]. Abbreviations: VAG = volcanic arc granites; ORG = ocean ridge granites; WPG = within-plate granites; syn-COLG = syn-collision granites; post-COLG = post-collision granites.

6. Conclusions

Through this study and the data compiled, we recognize that the Mesozoic magmatic rocks in Jiaodong Peninsula are adakitic rocks (inclu. Linglong, Guojialing, and Weideshan suites) and A-type granite (Laoshan suite). The adakitic rocks were mainly formed through partial melting of the thickened lower crust due to the subduction of the Paleo-Pacific Plate, and in the Early Cretaceous it was also mixed with a large amount of mantle material. The A1-type granite, represented by the Laoshan suite, was formed through partial melting of the crust with a small amount of mantle material. From the Jurassic to the Early Cretaceous, the tectonic and geochemical properties of magmatic rocks in Jiaodong Peninsula underwent significant changes. This transitional process, from compression to extension and reduction to oxidation, led to the formation of gold deposits.

Supplementary Materials: The following supporting information can be downloaded at: <https://www.mdpi.com/article/10.3390/min13081012/s1>, Table S1: LA-ICP-MS zircon U-Pb data for Laoshan granites from the Jiaodong Peninsula; Table S2: Major (wt.%) and trace element (ppm) data for Laoshan granitic intrusive rocks from the Jiaodong Peninsula; Table S3: Zircon trace element data for Laoshan granitic intrusive rocks from the Jiaodong Peninsula.

Author Contributions: Conceptualization, J.L. and M.S.; methodology, J.L., X.L. and C.W. (Changwei Wang); software, C.W. (Changjiang Wang) and S.L.; data curation, J.L., X.L. and Q.C.; investigation, J.L. and M.S.; project administration, M.S. All authors have read and agreed to the published version of the manuscript.

Funding: This research was funded by the “Shandong Natural Science Foundation, grant number ZR2021QD056” and the “National Natural Science Foundation of China-Shandong Joint Fund, grant number No. U2006201”.

Data Availability Statement: Data are contained within the Supplementary Materials.

Acknowledgments: We gratefully acknowledge the assistance of four anonymous reviewers for their insightful comments, which greatly improved the quality of this manuscript. We thank Fan Yang for his handling of the manuscript and editorial input. This work was financially supported by the Shandong Natural Science Foundation (No. ZR2021QD056) and the National Natural Science Foundation of China-Shandong Joint Fund (No. U2006201).

Conflicts of Interest: The authors declare no conflict of interest.

References

1. Song, M.C.; Li, J.; Yu, X.F.; Ding, Z.J.; Li, S.Y. Metallogenic characteristics and tectonic setting of the Jiaodong gold deposit, China. *Solid Earth Sci.* **2021**, *6*, 385–405. [[CrossRef](#)]
2. Song, M.C.; Song, Y.X.; Li, J.; Liu, H.B.; Li, J.; Dong, L.L.; He, C.Y.; Wang, R.S. Thermal doming-extension metallogenic system of Jiaodong type gold deposits. *Acta Petrol. Sin.* **2023**, *39*, 1241–1260, (In Chinese with English abstract). [[CrossRef](#)]
3. Deng, J.; Yang, L.Q.; Groves, D.I.; Zhang, L.; Qiu, K.F.; Wang, Q.F. An integrated mineral system model for the gold deposits of the giant Jiaodong province, eastern China. *Earth-Sci. Rev.* **2020**, *208*, 103274. [[CrossRef](#)]
4. Song, M.C.; Lin, S.Y.; Yang, L.Q.; Song, Y.X.; Ding, Z.J.; Li, J.; Li, S.Y.; Zhou, M.L. Metallogenic model of Jiaodong Peninsula gold deposits. *Miner. Depos.* **2020**, *39*, 215–236. (In Chinese with English abstract).
5. Yang, L.Q.; Deng, J.; Wang, Z.L.; Zhang, L.; Guo, L.N.; Song, M.C.; Zheng, X.L. Mesozoic gold metallogenic system of the Jiaodong gold province, eastern China. *Acta Petrol. Sin.* **2014**, *30*, 2447–2467. (In Chinese with English abstract).
6. Fan, H.R.; Feng, K.; Li, X.H.; Hu, F.F.; Yang, K.F. Mesozoic gold mineralization in the Jiaodong and Korean peninsulas. *Acta Petrol. Sin.* **2016**, *32*, 3225–3238. (In Chinese with English abstract).
7. Song, M.C.; Song, Y.X.; Ding, Z.J.; Li, S.Y. Jiaodong Gold Deposits: Essential Characteristics and Major Controversy. *Gold Sci. Technol.* **2018**, *26*, 406–422. (In Chinese with English abstract).
8. Zhu, R.X.; Fan, H.R.; Li, J.W.; Meng, Q.R.; Li, S.R.; Zeng, Q.D. Decratonic gold deposits. *Sci. China-Earth Sci.* **2015**, *58*, 1523–1537. [[CrossRef](#)]
9. Li, J.; Song, M.C.; Yu, J.T.; Bo, J.W.; Zhang, Z.L.; Liu, X. Genesis of Jinqingding Gold Deposit in eastern Jiaodong Peninsula, China: Constrains from trace elements of sulfide ore and wall-rock. *Geol. Bull. China* **2022**, *41*, 1010–1022. (In Chinese with English abstract).
10. Li, J.; Yang, Z.M.; Song, M.C.; Dong, L.L.; Li, S.Y.; Wang, R.S.; Liu, X.; Li, Z.S.; Song, Y.X.; Lai, C.K. Gold remobilization of the Sanshandao gold deposit, Jiaodong Peninsula, Eastern China: Perspective from in-situ sulfide trace elements and sulfur isotopes. *Ore Geol. Rev.* **2023**, *158*, 105505.
11. Li, J.; Dai, C.G.; Wang, C.W.; Song, M.C.; Wang, C.J.; Li, S.Y.; Wang, R.S.; Shi, H.J.; Xu, K.L.; Wang, P. Possible genetic relationship between Mesozoic magmatic rocks and gold mineralization in the Jiaodong Peninsula (Eastern China): Constraints of magmatic evolution and physicochemical conditions. *Front. Earth Sci.* **2023**; *under review*.
12. Yang, J.H.; Xu, L.; Sun, J.F.; Zeng, Q.D.; Zhao, Y.N.; Wang, H.; Zhu, Y.S. Geodynamics of decratonization and related magmatism and mineralization in the North China Craton. *Sci. China-Earth Sci.* **2021**, *64*, 1409–1427. [[CrossRef](#)]
13. Zhao, G.C.; Wilde, S.A.; Cawood, P.A.; Sun, M. Archean blocks and their boundaries in the North China Craton: Lithological, geochemical, structural and P-T, path constraints and tectonic evolution. *Precambrian Res.* **2001**, *107*, 45–73.
14. Zhao, G.C.; Sun, M.; Wilde, S.A.; Li, S.Z. Late Archean to Paleoproterozoic evolution of the North China Craton: Key issues revisited. *Precambrian Res.* **2005**, *136*, 177–202.
15. Yang, J.H.; Wu, F.Y. Triassic magmatism and its relation to decratonization in the eastern North China Craton. *Sci. China Ser. D-Earth Sci.* **2009**, *52*, 1319–1330.
16. Li, J.; Cai, W.Y.; Wang, K.Y.; Kim, N.H.; Liu, H.L.; Lee, J.G.; Yoo, B.C. Initial decratonization of the eastern North China Craton: New constraints from geochronology, geochemistry, and Hf isotopic compositions of Mesozoic igneous rocks in the Qingchengzi district. *Geol. J.* **2020**, *55*, 3796–3820.
17. Wu, F.Y.; Yang, J.H.; Xu, Y.G.; Wilde, S.A.; Walker, R.J. Destruction of the North China Craton in the Mesozoic. *Annu. Rev. Earth Planet. Sci.* **2019**, *47*, 173–195. [[CrossRef](#)]
18. Jahn, B.M.; Auvray, B.; Cornichet, J.; Bai, Y.L.; Shen, Q.H.; Liu, D.Y. 3.5 Ga old amphibolites from eastern Hebei province, China: Field occurrence, petrology, Sm–Nd isochron age and REE geochemistry. *Precambrian Res.* **1987**, *34*, 311–346.
19. Griffin, W.L.; O'Reilly, S.Y.; Ryan, C.G. Composition and thermal structure of the lithosphere beneath South Africa, Siberia and China: Proton microprobe studies. In Proceedings of the International Symposium on Cenozoic Volcanic Rocks and Deep-Seated Xenoliths of China and Its Environs, Beijing, China, 8–10 September 1992; pp. 65–66.

20. Griffin, W.L.; Zhang, A.; O'Reilly, S.Y.; Ryan, C.G. Phanerozoic evolution of the lithosphere beneath the Sino-Korean Craton. In *Mantle Dynamics and Plate Interactions in East Asia*; Geodynamics Series; Flower, M.F.J., Chung, S.-L., Lo, C.-H., Lee, T.-Y., Eds.; American Geophysical Union: Washington, DC, USA, 1998; Volume 27, pp. 107–126. [\[CrossRef\]](#)
21. Gao, S.; Rudnick, R.L.; Yuan, H.L.; Liu, X.M.; Liu, Y.S.; Xu, W.L.; Ling, W.L.; Ayers, J.; Wang, X.C.; Wang, Q.H. Recycling lower continental crust in the North China Craton. *Nature* **2004**, *432*, 892–897. [\[CrossRef\]](#)
22. Basu, A.R.; Wang, J.W.; Huang, W.K.; Xie, G.; Tatsumoto, M. Major element, REE, and Pb and Sr isotopic geochemistry of Cenozoic volcanic rocks of eastern China: Implications for their origin from suboceanic type mantle reservoirs. *Earth Planet. Sci. Lett.* **1991**, *105*, 149–169.
23. Menzies, M.A.; Fan, W.; Zhang, M. Paleozoic and Cenozoic lithoprobes and loss of N120 km of Archean lithosphere, Sino-Korean/Craton. *Magma. Process. Plate Tecton.* **1993**, *76*, 71–81.
24. Fan, W.M.; Zhang, H.F.; Baker, J.; Jarvis, K.E.; Mason, P.R.D.; Menzies, M.A. On and off the North China Craton: Where is the Archean keel? *J. Petrol.* **2000**, *41*, 933–950. [\[CrossRef\]](#)
25. Yang, J.H.; Wu, F.Y.; Wilde, S.A. A review of the geodynamic setting of large-scale Late Mesozoic gold mineralization in the North China Craton: An association with lithospheric thinning. *Ore Geol. Rev.* **2003**, *23*, 125–152.
26. Dong, L.L.; Yang, Z.M.; Song, M.C.; Bai, X. Petrogenesis of Mesozoic Magmatic Suites in the Jiaodong Peninsula: Implications for Crust-Mantle Interactions and Decratonization. *Lithosphere* **2023**, *2023*, 6226908.
27. Song, M.C.; Zhou, J.B.; Song, Y.X.; Wang, B.; Li, S.Y.; Li, J.; Wang, S.S. Mesozoic Weideshan granitoid suite and its relationship to large-scale gold mineralization in the Jiaodong Peninsula, China. *Geol. J.* **2020**, *55*, 5703–5724. [\[CrossRef\]](#)
28. Paton, C.; Woodhead, J.D.; Hellstrom, J.C.; Hergt, J.M.; Greig, A.; Maas, R. Improved laser ablation U-Pb zircon geochronology through robust downhole fractionation correction. *Geochem. Geophys. Geosyst.* **2010**, *11*, Q0AA06. [\[CrossRef\]](#)
29. Ludwig, K.R. User's manual for isoplot 3.0: A geochronological toolkit for Microsoft Excel. *Berkeley Geochronol. Cent. Spec. Publ.* **2003**, *4*, 25–32.
30. Andersen, T. Correction of common lead in U-Pb analyses that do not report ²⁰⁴Pb. *Chem. Geol.* **2002**, *192*, 59–79. [\[CrossRef\]](#)
31. Hoskin, P.W.O.; Black, L.P. Metamorphic zircon formation by solid-state recrystallization of protolith igneous zircon. *J. Metamorph. Geol.* **2000**, *18*, 423–439. [\[CrossRef\]](#)
32. Hoskin, P.W.O. Trace-element composition of hydrothermal zircon and the alteration of hadean zircon from the Jack Hills, Australia. *Geochim. Cosmochim. Acta* **2005**, *69*, 637–648. [\[CrossRef\]](#)
33. Irvine, T.H.; Baragar, W.R.A. A guide to the chemical classification of the common volcanic rocks. *Can. J. Earth Sci.* **1971**, *8*, 523–548. [\[CrossRef\]](#)
34. Peccerillo, A.; Taylor, D.R. Geochemistry of Eocene calc-alkaline volcanic rocks from the Kastamonu area, northern Turkey. *Contrib. Mineral. Petrol.* **1976**, *58*, 63–81. [\[CrossRef\]](#)
35. Maniar, P.D.; Piccoli, P.M. Tectonic discrimination of granitoids. *Geol. Soc. Am. Bull.* **1989**, *101*, 635–643. [\[CrossRef\]](#)
36. Hou, M.L.; Jiang, Y.H.; Jiang, S.Y.; Ling, H.F.; Zhao, K.D. Contrasting origins of late mesozoic adakitic granitoids from the northwestern, Jiaodong Peninsula, east China: Implications for crustal thickening to delamination. *Geol. Mag.* **2007**, *144*, 619–631.
37. Li, X.C.; Fan, H.R.; Santosh, M.; Hu, F.F.; Yang, K.F.; Lan, T.G.; Liu, Y.; Yang, Y.H. An evolving magma chamber within extending lithosphere: An integrated geochemical, isotopic and zircon U-Pb geochronological study of the Gushan granite, eastern North China Craton. *J. Asian Earth Sci.* **2012**, *50*, 27–43.
38. Yang, K.F.; Fan, H.R.; Santosh, M.; Hu, F.F.; Wilde, S.; Lan, T.G.; Lu, L.N.; Liu, Y.S. Reactivation of the Archean lower crust: Implications for zircon geochronology, elemental and Sr-Nd-Hf isotopic geochemistry of late Mesozoic granitoids from northwestern Jiaodong Terrane, the North China Craton. *Lithos* **2012**, *146*, 112–127.
39. Ma, L.; Jiang, S.Y.; Dai, B.Z.; Jiang, Y.H.; Hou, M.L.; Pu, W.; Bin, X. Multiple sources for the origin of Late Jurassic Linglong adakitic granite in the Shandong Peninsula, eastern China: Zircon U-Pb geochronological geochemical and Sr-Nd-Hf isotopic evidence. *Lithos* **2013**, *162*, 175–194.
40. Yan, Q.S.; Shi, X.F. Geochemistry and petrogenesis of the Cretaceous A-type granites in the Laoshan granitic complex, eastern China. *Isl. Arc* **2014**, *23*, 221–235. [\[CrossRef\]](#)
41. Gao, Y.J.; Niu, Y.L.; Duan, M.; Xue, Q.Q.; Sun, P.; Chen, S.; Xiao, Y.Y.; Guo, P.Y.; Wang, X.H.; Chen, Y.H. The petrogenesis and tectonic significance of the Early Cretaceous intraplate granites in eastern China: The Laoshan granite as an example. *Lithos* **2019**, *328–329*, 200–211.
42. Li, X.H.; Fan, H.R.; Hu, F.F.; Hollings, P.; Yang, K.F.; Liu, X. Linking lithospheric thinning and magmatic evolution of Late Jurassic to Early Cretaceous granitoids in the Jiaobei Terrane, southeastern North China Craton. *Lithos* **2019**, *324–325*, 280–296. [\[CrossRef\]](#)
43. He, J.T. Gold Mineralization and Post Ore Enrollment in the Muping Rushan Gold Belt, Jiaodong Peninsula, Eastern China. Ph.D. Thesis, China University of Geosciences, Beijing, China, 2021; pp. 1–171. (In Chinese with English abstract).
44. Wang, B.; Song, M.C.; Huo, G.; Zhou, M.L.; Xu, Z.H.; Jiang, L.; Song, Y.X.; Li, J. Source characteristics and tectonic evolution of Late mesozoic granites in Jiaodong and their implications for gold mineralization. *Acta Petrol. Mineral.* **2021**, *40*, 288–320. (In Chinese with English abstract).
45. Dong, L.L.; Yang, Z.M.; Bai, X.; Deng, C. Generation of the Early Cretaceous granitoid in the Dazeshan region, Jiaodong Peninsula: Implications for the crustal reworking in the North China Craton. *Front. Earth Sci.* **2023**, *10*, 1083608. [\[CrossRef\]](#)
46. Wang, D.; Wang, T.Q.; Li, H.Y. Petrogenesis of Early Cretaceous Laoshan A-type granites and the implications for the tectonic evolution of Jiaodong Peninsula. *Acta Petrol. Sin.* **2023**, *39*, 317–339. (In Chinese with English abstract). [\[CrossRef\]](#)

47. McDonough, W.F.; Sun, S.S. The composition of the Earth. *Chem. Geol.* **1995**, *120*, 223–253. [[CrossRef](#)]
48. Richards, J.P. Tectono-magmatic precursors for porphyry Cu–(Mo–Au) deposit formation. *Econ. Geol.* **2003**, *98*, 1515–1533.
49. Richards, J.P. High Sr/Y arc magmas and porphyry Cu Mo Au deposits: Just add water. *Econ. Geol.* **2011**, *106*, 1075–1081.
50. Richards, J.P.; Kerrich, R. Special paper: Adakite-like rocks: Their diverse origins and questionable role in metallogenesis. *Econ. Geol.* **2007**, *102*, 537–576.
51. Moyen, J.F. High Sr/Y and La/Yb ratios: The meaning of the “adakitic signature”. *Lithos* **2009**, *112*, 556–574. [[CrossRef](#)]
52. Cai, W.Y.; Wang, K.Y.; Li, J.; Fu, L.J.; Lai, C.K.; Liu, H.L. Geology, geochronology and geochemistry of large Duobaoshan Cu–Mo–Au orefield in NE China: Magma genesis and regional tectonic implications. *Geosci. Front.* **2021**, *12*, 265–292.
53. Martin, H. Effect of steeper Archean geochemical gradient on geochemistry of subduction-zone magmas. *Geology* **1986**, *14*, 753–756. [[CrossRef](#)]
54. Defant, M.J.; Drummond, M.S. Derivation of some modern arc magmas by melting of young subducted lithosphere. *Nature* **1990**, *347*, 662–665. [[CrossRef](#)]
55. Martin, H. Petrogenesis of Archean trondhjemites, tonalities and granodiorites from eastern Finland: Major and trace element geochemistry. *J. Petrol.* **1987**, *28*, 921–953. [[CrossRef](#)]
56. Drummond, M.S.; Defant, M.J.; Kepezhinskas, P.K. Petrogenesis of slab-derived trondhjemite–tonalite–dacite/adakite magmas. In *Third Hutton Symposium on the Origin of Granites and Related Rocks*; Special Paper; Brown, M., Candela, P.A., Peckert, D.L., Eds.; Geological Society of America: Boulder, CO, USA, 1996; Volume 315, pp. 205–215.
57. Martin, H.; Smithies, R.H.; Rapp, R.; Moyen, J.F.; Champion, D.C. An overview of adakite, tonalite–trondhjemite–granodiorite (TTG), and sanukitoid: Relationships and some implications for crustal evolution. *Lithos* **2005**, *79*, 1–24.
58. Gao, S.; Luo, T.C.; Zhang, B.R.; Zhang, H.F.; Han, Y.W.; Zhao, Z.D.; Hu, Y.K. Chemical composition of the continental crust as revealed by studies in East China. *Geochim. Cosmochim. Acta* **1998**, *62*, 1959–1975. [[CrossRef](#)]
59. Chappell, B.W.; White, A.J.R. Two contrasting granite types: 25 years later. *Aust. J. Earth Sci.* **2001**, *48*, 489–499. [[CrossRef](#)]
60. Taylor, S.R.; McLennan, S.M. *The Continental Crust: Its Composition and Evolution*; Oxford Press: Blackwell, UK, 1985; p. 312.
61. Rudnick, R.L.; Gao, S.; Ling, W.L.; Liu, Y.S.; McDonough, W.F. Petrology and geochemistry of spinel peridotite xenoliths from Hannuoba and Qixia, North China Craton. *Lithos* **2004**, *77*, 609–637. [[CrossRef](#)]
62. Hofmann, A.W.; Jochum, K.P.; Seufert, M.; White, W.M. Nb and Pb in oceanic basalts: New constraints on mantle evolution. *Earth Planet. Sci. Lett.* **1986**, *79*, 33–45. [[CrossRef](#)]
63. Rapp, R.P.; Shimizu, N.; Norman, M.D.; Applegate, G.S. Reaction between slab derived melts and peridotite in the mantle wedge: Experimental constraints at 3.8 GPa. *Chem. Geol.* **1999**, *160*, 335–356.
64. Ji, Z.; Ge, W.C.; He, Y.; Bi, J.H.; Dong, Y.; Yang, H.; Hao, Y.J. Mixing of cognate magmas as a process for producing high-silica granites: Insights from Guanmenshan Complex in Liaodong Peninsula, China. *Lithos* **2021**, *406–407*, 106495.
65. Stern, C.R.; Kilian, R. Role of the subducted slab, mantle wedge and continental crust in the generation of adakites from the Austral Volcanic Zone. *Contrib. Mineral. Petrol.* **1996**, *123*, 263–281.
66. Martin, H. Adakitic magmas: Modern analogues of Archean granitoids. *Lithos* **1999**, *46*, 411–429. [[CrossRef](#)]
67. Smithies, R.H. The Archean tonalite–trondhjemite–granodiorite (TTG) series is not an analogue of Cenozoic adakite. *Earth Planet. Sci. Lett.* **2000**, *182*, 115–125. [[CrossRef](#)]
68. Defant, M.J.; Xu, J.F.; Kepezhinskas, P.; Wang, Q.; Zhang, Q.; Xiao, L. Adakites: Some variations on a theme. *Acta Petrol. Sin.* **2002**, *18*, 129–142.
69. Atherton, M.P.; Petford, N. Generation of sodium-rich magmas from newly underplated basaltic crust. *Nature* **1993**, *362*, 144–146. [[CrossRef](#)]
70. Petford, N.; Atherton, M. Na-rich partial melts from newly underplated basaltic crust: The Cordillera Blanca Batholith, Peru. *J. Petrol.* **1996**, *37*, 1491–1521.
71. Muir, R.J.; Weaver, S.D.; Bradshaw, J.D.; Eby, G.N.; Evans, J.A. Geochemistry of the Cretaceous Separation Point Batholith, New Zealand: Granitoid magmas formed by melting of mafic lithosphere. *J. Geol. Soc.* **1995**, *152*, 689–701.
72. Xu, J.F.; Shinjo, R.; Defant, M.J.; Wang, Q.; Papp, R.P. Origin of Mesozoic adakitic intrusive rock in the Ningzhen area of east China: Partial melting of delaminated lower continental crust? *Geology* **2002**, *30*, 1111–1114. [[CrossRef](#)]
73. Woodhead, J.D.; Eggins, S.M.; Johnson, R.W. Magma genesis in the New Britain island arc: Further insights into melting and mass transfer processes. *J. Petrol.* **1998**, *39*, 1641–1668.
74. Kepezhinskas, P.; McDermott, F.; Defant, M.J.; Hochstaedter, A.; Drummond, M.S.; Hawkesworth, C.J.; Koloskov, A.; Maury, R.C.; Bellon, H. Trace element and SrNd–Pb isotopic constraints on a three-component model of Kamchatka Arc petrogenesis. *Geochim. Cosmochim. Acta* **1997**, *61*, 577–600. [[CrossRef](#)]
75. Whalen, J.B. Geochemistry of an island-arc plutonic suite: The Uasilau–Yau Yau intrusive complex, New Britain P.N.G. *J. Petrol.* **1985**, *26*, 603–632. [[CrossRef](#)]
76. Watson, E.B.; Harrison, T.M. Zircon saturation revisited: Temperature and composition effects in a variety of crustal magma types. *Earth Planet. Sci. Lett.* **1983**, *64*, 295–304. [[CrossRef](#)]
77. Li, J.; Wang, K.Y.; Fu, L.J.; Zhang, M.; Liu, H.L.; Liu, Q.Z.; Tang, W.H.; Wang, C.H. Adakitic rocks and A-type felsic dykes in the Changlingzi area, NE China: Constraints on multistage tectonism in the southern Great Xing’an Range. *Geol. J.* **2020**, *55*, 5451–5478. [[CrossRef](#)]

78. Pearce, J.A. Role of the sub-continental lithosphere in magma genesis at active continental margins. In *Continental Basalts and Mantle Xenoliths*; Hawkesworth, C.J., Norry, M.J., Eds.; Shiva Press: Nantwich, UK, 1983; pp. 230–249.
79. Tischendorf, G.; Paelchen, W. On the classification of granitoids. *Z. Fuer Geol. Wiss.* **1985**, *13*, 615–627.
80. Wilson, M. *Igneous Petrogenesis a Global Tectonic Approach*; Unwin Hyman: London, UK, 1989; p. 466.
81. Whalen, J.B.; Currie, K.L.; Chappell, B.W. A-type granites: Geochemical characteristics, discrimination and petrogenesis. *Contrib. Mineral. Petrol.* **1987**, *95*, 407–419.
82. Eby, G.N. Chemical subdivision of the A-type granitoids: Petrogenetic and tectonic implications. *Geology* **1992**, *20*, 641–644. [[CrossRef](#)]
83. Qian, Q.; Zhong, S.L.; Li, T.Y.; Wen, D.R. Geochemical characteristics and petrogenesis of the Badaling high Ba–Sr granitoids: A comparison of igneous rocks from North China and the Dabie–Sulu Orogen. *Acta Petrol. Sin.* **2002**, *18*, 275–292. (In Chinese with English abstract).
84. Shu, Q.H.; Chang, Z.S.; Lai, Y.; Hu, X.L.; Wu, H.Y.; Zhang, Y.; Wang, P.; Zhai, D.G.; Zhang, C. Zircon trace elements and magma fertility: Insights from porphyry (–skarn) Mo deposits in NE China. *Miner. Depos.* **2019**, *54*, 645–656.
85. Li, Y.; Audétat, A. Partitioning of V, Mn Co, Ni, Cu, Zn, As, Mo, Ag, Sn, Sb, W, Au, Pb, and Bi between sulfide phases and hydrous basanite melt at upper mantle conditions. *Earth Planet Sci. Lett.* **2012**, 355–356, 327–340. [[CrossRef](#)]
86. Sun, W.D.; Liang, H.Y.; Ling, M.X.; Zhan, M.Z.; Ding, X.; Zhang, H.; Yang, X.Y.; Li, Y.L.; Ireland, T.R.; Wei, Q.R.; et al. The link between reduced porphyry copper deposits and oxidized magmas. *Geochim. Cosmochim. Acta* **2013**, *103*, 263–275. [[CrossRef](#)]
87. Williams-Jones, A.E.; Bowtell, R.J.; Migdisov, A.A. Gold in solution. *Elements* **2009**, *5*, 281–287. [[CrossRef](#)]
88. Loucks, R.R.; Fiorentini, M.L.; Henriquez, G.J. New magmatic oxybarometer using trace elements in zircon. *J. Petrol.* **2020**, *61*, ega034. [[CrossRef](#)]
89. Trail, D.; Bruce Watson, E.; Tailby, N.D. Ce and Eu anomalies in zircon as proxies for the oxidation state of magmas. *Geochim. Cosmochim. Acta* **2012**, *97*, 70–87. [[CrossRef](#)]
90. Rezeau, H.; Moritz, R.; Wotzlaw, J.F.; Hovakimyan, S.; Tayan, R. Zircon Petrochronology of the Meghri-Ordubad Pluton, Lesser Caucasus: Fingerprinting Igneous Processes and Implications for the Exploration of Porphyry Cu–Mo Deposits. *Econ. Geol.* **2019**, *114*, 1365–1388.
91. Dong, L.L.; Yang, Z.M.; Liu, Y.H.; Song, M.C. Possible source of Au in the Jiaodong area from lower crustal sulfide cumulates: Evidence from oxygen states and chalcophile elements contents of Mesozoic magmatic suites. *Ore Geol. Rev.* **2023**, *153*, 105268.
92. Goss, C.S.; Wilde, S.A.; Wu, F.Y.; Yang, J.H. The age, isotopic signature and significance of the youngest Mesozoic granitoids in the Jiaodong Terrane. Shandong Province. North China Craton. *Lithos* **2010**, *120*, 309–326. [[CrossRef](#)]
93. Yan, Q.S.; Metcalfe, I.; Shi, X.F.; Zhang, P.Y.; Li, F.C. Early Cretaceous granitic rocks from the southern Jiaodong Peninsula eastern China: Implications for lithospheric extension. *Int. Geol. Rev.* **2019**, *61*, 821–838.
94. Cai, W.Y.; Wang, Z.G.; Li, J.; Fu, L.J.; Wang, K.Y.; Yasssa, K.; Li, S.D. Zircon U–Pb and molybdenite Re–Os geochronology and geochemistry of Jinchang porphyry gold–copper deposit, NE China: Two-phase mineralization and the tectonic setting. *Ore Geol. Rev.* **2019**, *107*, 735–753.
95. Yang, F.; Santosh, M.; Kim, S.W. Mesozoic magmatism in the eastern North China Craton: Insights on tectonic cycles associated with progressive craton destruction. *Gondwana Res.* **2018**, *60*, 153–178.
96. Yang, F.; Santosh, M.; Glorie, S.; Jepson, G.; Xue, F.; Kim, S.W. Meso-Cenozoic multiple exhumation in the Shandong Peninsula, eastern North China Craton: Implications for lithospheric destruction. *Lithos* **2020**, 370–371, 105597.
97. Groves, D.I.; Goldfarb, R.J.; Gebre-Mariam, M.; Hagemann, S.G.; Robert, F. Orogenic gold deposits: A proposed classification in the context of their crustal distribution and relationship to other gold deposit types. *Ore Geol. Rev.* **1998**, *13*, 7–27.
98. Pearce, J.A.; Harris, N.B.W.; Tindle, A.G. Trace element discrimination diagrams for the tectonic interpretation of granitic rocks. *J. Petrol.* **1984**, *25*, 956–983. [[CrossRef](#)]
99. Pearce, J.A.; Peate, D.W. Tectonic implications of the composition of volcanic arc magmas. *Annu. Rev. Earth Planet Sci.* **1995**, *23*, 251–285. [[CrossRef](#)]
100. Harris, R.A.; Stone, D.B.; Turner, D.L. Tectonic implications of paleomagnetic and geochronologic data from the Yukon-Koyukuk province, Alaska. *Geol. Soc. Am. Bull.* **1987**, *99*, 362–375. [[CrossRef](#)]

Disclaimer/Publisher’s Note: The statements, opinions and data contained in all publications are solely those of the individual author(s) and contributor(s) and not of MDPI and/or the editor(s). MDPI and/or the editor(s) disclaim responsibility for any injury to people or property resulting from any ideas, methods, instructions or products referred to in the content.